Cai et al. *Quantum Frontiers* (2026) 5:1
https://doi.org/10.1007/s44214-025-00098-0

Quantum Frontiers

REVIEW Open Access

Emergent phenomena in kagome thin films: a spectroscopic perspective

Yongqing Cai[1,2], Vladimir Vasilyevich Uglov[3,4], Jijun Zhao[5,6] and Huimin Zhang[1,2,3*]

Abstract

Kagome materials have recently emerged as a versatile platform for exploring the intricate interplay among lattice, charge, spin, and orbital degrees of freedom, giving rise to a rich variety of quantum phenomena. While early studies predominantly focused on bulk kagome crystals, recent efforts have increasingly shifted toward their thin-film counterparts, motivated by the pursuit of enhanced tunability and potential device integration. Compared to bulk crystals, thin films offer distinct advantages such as precise control over strain, substrate-induced interactions, and reduced dimensionality, which together enable the modulation of electronic structures and the stabilization of emergent states. In particular, the ability to fine-tune key band features relative to the Fermi level provides a powerful route for engineering exotic states, including flat-band-driven magnetism, topological phases, and correlated electron phenomena. In this review, we provide a comprehensive overview of recent advances in the synthesis, characterization, and electronic structure studies of kagome thin films. We highlight key experimental breakthroughs that reveal how their topological and correlated properties evolve and discuss their broader significance within the landscape of quantum materials. Given the rapid convergence of experimental observations across diverse kagome systems, this review aims to offer timely guidance for future efforts toward unraveling the microscopic mechanisms of these unconventional electronic states.

Keywords: Kagome films, Flat bands, Dirac cone, Scanning tunneling microscopy, Angle-resolved photoemission spectroscopy

1 Introduction

The kagome lattice, consisting of a two-dimensional (2D) network of corner-sharing triangles, is a remarkable structural motif that hosts a wide spectrum of exotic quantum phenomena [1–4]. In this geometry, each vertex is shared by three triangles, forming an interconnected network of both nearest-neighbor and next-nearest-neighbor interactions (Fig. 1(a)). For the antiferromagnetic Heisenberg model on a triangular sublattice, no unique ground state can simultaneously satisfy all antiferromagnetic correlation interactions, resulting in spin frustration. Moreover, eigenfunctions at adjacent corners exhibit opposite phases, leading to phase cancellation for hopping between neighboring sites (indicated by black arrows in Fig. 1(b)). As a consequence, electronic states become geometrically confined within individual hexagons, a real-space localization that gives rise to a topological flat band with quenched kinetic energy. Based on a simple *s*-orbital tight-binding model with nearest-neighbor hopping, the inherent geometric frustration and symmetry give rise to distinctive electronic features such as Dirac cones, flat bands, and van Hove singularities (Fig. 1(c)) [5]. These characteristics stem from the intricate interplay among lattice, charge, spin and orbital degrees of freedom, positioning

*Correspondence: huiminzhang@dlut.edu.cn
[1]Key Laboratory of Materials Modification by Laser, Ion and Electron Beams (Dalian University of Technology), Ministry of Education, School of Physics, Dalian 116024, China
[2]Department of Physics, Dalian University of Technology, Dalian 116024, China
Full list of author information is available at the end of the article

Springer

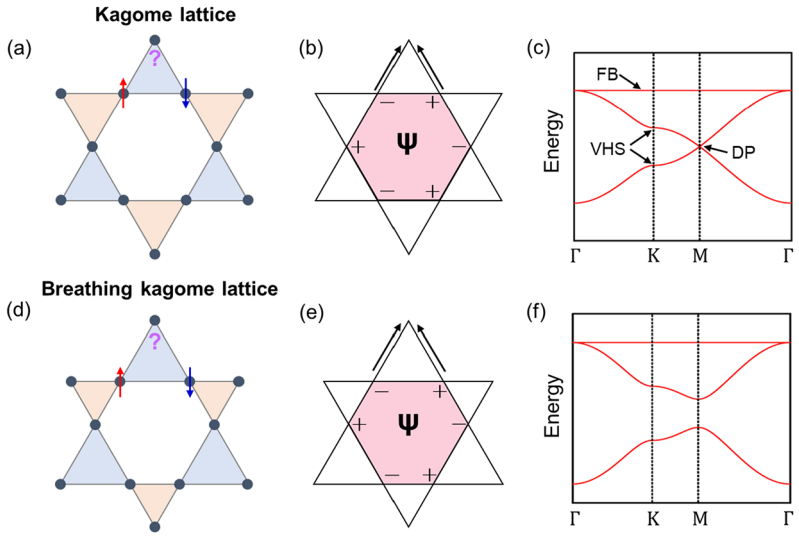

Figure 1 Kagome lattice and its characteristic band structure. (a) Schematic illustration of the regular kagome lattice structure. (b) Schematic of destructive interference of Bloch wave functions (ψ) in the kagome lattice. Electrons are confined within the pink-shaded hexagons due to destructive interference, as indicated by the black arrows. (c) Topological band structure of the kagome lattice considering nearest-neighbor electron hopping. The van Hove singularity (VHS), Dirac point (DP), and flat band (FB) are labeled. (d–f) Same as (a)–(c), but for the breathing kagome lattice

kagome materials as a fertile platform for investigating strongly correlated and topological quantum states [6–8]. In a more general scenario, when the shared triangles (marked by light brown and blue) differ in size or interaction strength, the lattice evolves into a breathing kagome structure (Figs. 1(d)–(f)), which introduces additional structural complexity and modifies the corresponding band dispersion relations. This inequivalence lifts the degeneracy of the two originally overlapping Dirac bands, thereby opening a band gap at the Dirac cone.

A defining aspect of kagome materials is the simultaneous emergence of multiple intertwined quantum phenomena. By tuning its filling in the kagome lattice, flat band can generate non-trivial topological states [9–11], nematic phases [12, 13], ferromagnetism with spin-polarized bands [14, 15] and Wigner crystallization [15, 16]. Van Hove singularities generate a high density of states that amplifies electron correlations, thereby promoting strong Fermi-surface nesting and associated instabilities [17, 18]. Meanwhile, Dirac cones host relativistic quasiparticles and topological surface states, enabling phenomena such as the quantum spin Hall effect [5] and dissipationless chiral edge modes [19], with promising implications for spintronics and quantum information technologies.

Kagome materials encompass extensive compositions and magnetic ground states, ranging from ferromagnetic and antiferromagnetic to nonmagnetic systems. In ferromagnetic kagome metals, $Co_3Sn_2S_2$ hosts magnetic Weyl fermions and a chiral anomaly [20, 21], Fe_3Sn_2 features massive Dirac fermions [22] accompanied by signatures of magnetic skyrmions [23], and $TbMn_6Sn_6$ exhibits Chern-gapped Dirac fermions [19]. Among antiferromagnetic systems, FeSn displays Dirac points and flat bands [24], FeGe reveals the coexistence of canted antiferromagnetic order and charge density wave (CDW) states [25–27], while Mn_3Sn and Mn_3Ge are characterized by chiral spin structures [28, 29]. A particular example is the layered AV_3Sb_5 (A = K, Rb, Cs) [30–32], which has recently attracted intense interest due to its unconventional electronic orders, including giant anomalous Hall conductivity [33, 34], pair density wave [35], CDW [36], electronic nematicity [37, 38], time reversal symmetry breaking [39–41] and possible chiral flux phase [45]. These exotic properties of kagome materials are illustrated in Fig. 2. A systematic comparison across different kagome families promises to yield deeper insights into the interplay between topology and electron correlations within the kagome framework.

In recent years, research focus has shifted remarkably from bulk kagome crystals to their thin-film counterparts. Compared with bulk systems, thin films offer several distinct advantages. They enable the application of external control parameters such as strain and substrate interactions, thereby tuning the electronic structure and stabilizing novel quantum states. They also facilitate integration into device architectures, bridging fundamental studies with potential applications in quantum technology. Furthermore, thin films provide access to emergent phenomena associated with the dimensional crossover from three to two dimensions. Despite these opportunities, kagome thin films also pose significant challenges in sample growth and characterization. For van der Waals (vdW)

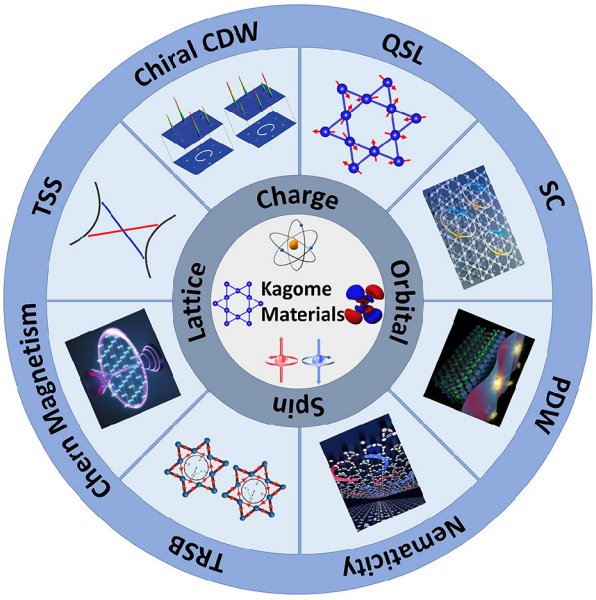

Figure 2 Exotic physical properties of Kagome materials. Note: TSS, topological surface state; QSL, quantum spin liquid; SC, superconductivity; PDW, pair density wave; TRSB, time-reversal symmetry breaking [1]; Chern magnetism [19]; Chiral CDW [36]. SC, reproduced with permission from Ref. [42]; image credit: Paul Scherrer Institute. PDW, reproduced with permission from Ref. [43]; image credit: Brookhaven National Laboratory. Nematicity, reproduced with permission from Ref. [44]; image credit: University of Science and Technology of China

kagome compounds, thin films can be prepared by mechanical exfoliation [46–49]. In contrast, fabricating high-quality non-vdW kagome films with controlled stoichiometry, smooth surfaces, and minimal defects requires advanced techniques such as molecular beam epitaxy (MBE) and magnetron sputtering. Probing their complex electronic structures further demands state-of-the-art methods, particularly scanning tunneling microscopy/spectroscopy (STM/S) to direct access to local density of states at the atomic scale, and angle-resolved photoemission spectroscopy (ARPES) to unravel the electronic structures.

This review focuses on recent progress in synthesis, characterization and electronic structure studies of kagome thin films. We first examine state-of-the-art thin-film growth techniques and strategies for achieving high-quality kagome films. Subsequently, we will delve into STM and ARPES investigations, highlighting their role in unraveling the intrinsic electronic properties and quantum phenomena of kagome thin films. Finally, we will explore the potential applications of these materials and provide insights into future directions for research. By synthesizing the current state of knowledge, this review aims to provide a coherent overview and inspire further exploration of kagome thin films as a promising frontier in quantum materials research.

2 Growth strategies for kagome thin films

The synthesis of high-quality thin films is a prerequisite for probing the quantum phenomena discussed above. Here we summarize the principal synthesis approaches and their implications for material properties (Table 1).

Binary kagome compounds T_mX_n (T = Mn, Fe, Co; X = Sn, Ge; m:n = 3:1, 3:2, 1:1) have attracted considerable attention owing to the coexistence of topological band crossings and flat bands originating from their kagome metal sublattices [22, 24, 28, 50–55]. Among these, FeSn has been the focus of early thin-film studies [56–63]. MBE enables the growth of single-phase FeSn films on perovskite oxide substrates including $SrTiO_3$ and $LaAlO_3$. Typically, FeSn films grown on $LaAlO_3$(111) and $SrTiO_3$(111) form discrete islands of 20-200 nm [57, 60], while continuous films have also been obtained on $SrTiO_3$(111) [56]. Magnetron sputtering with Pt or Ru buffer layers provides an alternative epitaxial route [64], though the strong spin–orbit coupling of Pt complicates studies of intrinsic spin–orbit torques in FeSn [65]. A more recent work has demonstrated continuous epitaxial films on Co or Fe underlayers by MBE [61], opening pathways for device integration.

For flat-band kagome metals such as CoSn, fine-tuning the flat band position relative to the Fermi level is vital, since many exotic physical properties are governed by states around the Fermi level. Epitaxial CoSn thin films have been grown on metallic buffer layers by sputtering [85], while more recently, a three-step MBE process enabled epitaxy on insulating MgO(111) and 4H-SiC(0001) substrates [68], providing a promising platform for flat-band physics and electrostatic control. Fe_3Sn_2 thin films are reported to host tunable Weyl fermions and large anomalous Hall and Nernst effects [81]. MBE-grown bilayer Fe_3Sn_2(0001)/Pt(111) (5/5 nm) films on Al_2O_3(0001) substrates have demonstrated strong spin–orbit torque responses, facilitating the development of spintronics based on topological kagome magnets [105]. In parallel, buffer-free epitaxial Fe_3Sn_2 films have been synthesized on Al_2O_3 (0001) and MgO(111) using facing-target magnetron sputtering [83], highlighting the diversity of viable approaches.

Beyond these prototypical cases, other kagome metals have also been realized in thin-film form, including RMn_6Sn_6 (R = rare earth)[71], $Co_3Sn_2S_2$ [84], Ni_3In [72], Mn_3Ge [73, 87], Mn_3Ga [89], $Gd_xYb_{1-x}Pb_3$/Si(111) [74], Ni/Pb(111) [75], Ge/Al(111) [76], Ag/Si(111) [77], and CsV_3Sb_5 [90, 91]. Layered kagome semiconductors such as $Pd_3P_2S_8$, Nb_3Cl_8, and Nb_3I_8 can be readily cleaved into ultrathin flakes owing to their weak vdW bonding. In contrast, non-vdW kagome semiconductors, such as SiO_2/Au(111) [92], FeSb [93], Cr_8Se_{12} [94] and silicene/Ag(111) [95], require epitaxial growth by MBE. Another distinct direction is the construction of artificial kagome lattices through supramolecular self-assembly. Organic molecular building blocks deposited on noble-metal substrates have enabled precise kagome networks,

Table 1 Methods for synthesizing kagome materials

	Molecular beam epitaxy	Magnetic sputtering	Mechanical exfoliation
Metal	FeSn [56–63, 66], Fe_3Sn_2 [67], CoSn [68, 69], FeGe [70], RMn_6Sn_6 [71], Ni_3In [72], Mn_3Ge [73], $Gd_xYb_{1-x}Pb_3$/Si(111) [74], Ni/Pb(111) [75], Ge/Al(111) [76], Ag/Si(111) [77]	Fe_3Sn [78–80], Fe_3Sn_2 [81–83], $Co_3Sn_2S_2$ [84], CoSn [85], FeSn [86], Mn_3Ge [87], Mn_3Sn [53, 88], Mn_3Ga [89]	CsV_3Sb_5 [90, 91]
Semiconductor	SiO_2/Au(111) [92], FeSb [93], Cr_8Se_{12} [94], silicene/Ag(111) [95], $MoTe_2$ [96]	\	$Pd_3P_2S_8$ [97]
Mott insulator	\	\	Nb_3I_8 [47], Nb_3Cl_8 [46, 98]
Organic molecule	P^2TANGO/Au(111) [99], porphyrin/Au(111) [100], B2-Per/Ag(111) [101], NC-Ph_5-CN/Ag(111) [102], benzene/Br/Ag(111) [103], P^2TANG/Au(111) [104]	\	\

including porphyrin-, perylene-, and benzene-based lattices [99–104, 106]. These supramolecular assemblies represent a versatile strategy to engineer desired kagome electronic states with atomic precision.

The choice of synthesis method is critical, as it directly determines the structural quality, scalability, and functional properties of the kagome thin film. MBE excels in delivering atomically precise, stoichiometrically controlled epitaxial films with ultra-high purity and sharp interfaces, making it ideal for fundamental studies of electronic structure and interfacial phenomena. However, its ultrahigh vacuum requirements, low growth rates, and high operational cost limit throughput and large-area fabrication. Magnetron sputtering offers a more scalable and cost-effective route, capable of depositing uniform films over larger substrates at higher deposition rates. It is particularly suitable for growing polycrystalline or textured films of multi-element compounds. Challenges include achieving the same level of epitaxial perfection as MBE and potentially introducing higher defect densities or off-stoichiometry. For layered vdW kagome materials, mechanical exfoliation provides a straightforward method to isolate ultrathin flakes, preserving the intrinsic crystalline quality of the bulk. This method is invaluable for rapidly prototyping devices and exploring thickness-dependent properties down to the monolayer limit. Its principal limitations are the lack of control over flake size, thickness, and lateral uniformity, as well as the inability to create heterostructures with atomically clean interfaces in a controlled manner. Each technique thus presents a distinct trade-off between crystalline perfection, scalability, and experimental versatility, guiding the selection based on the specific scientific or application purpose.

3 STM studies: local electronic structures and surface states

STM/STS provide atomic-scale insights into the real-space electronic properties of kagome materials, complementing momentum-resolved techniques like ARPES. This section synthesizes key STM/STS findings on kagome thin films, highlighting defect engineering, topological states, and correlation-driven phenomena.

3.1 Engineering electronic states in FeSn and Fe_3Sn_2 kagome films

Strain engineering has emerged as a powerful strategy for manipulating Dirac fermions in topological materials, owing to their high sensitivity to lattice distortions [107]. A compelling example is provided by epitaxial FeSn films, in which the weak bonding of the stanene sublattice makes the structure particularly susceptible to strain. The model kagome magnet FeSn consists of alternatingly stacked 2D Fe_3Sn kagome and Sn honeycomb layers (Fig. 3(a)) [60]. STM measurements reveal that ultrathin films develop periodic stripe-like modulations in the Sn honeycomb lattice (Fig. 3(b)), reflecting strain-induced lattice distortions. These modulations strongly impact the low-energy electronic states: spatially resolved dI/dV spectra show highly regular oscillations that repeat over successive stripes (Fig. 3(c)). More strikingly, differential conductance measurements on and between the stripes resolve a series of discrete peaks (Fig. 3(d)), identified as Landau levels arising from pseudomagnetic fields generated by the strain. Quantitative analysis indicates that the effective field exceeds 1000 T, placing it among the largest pseudomagnetic fields reported in Dirac systems.

The implications of this finding are twofold. First, it establishes kagome metals as an exceptional platform where modest lattice distortions can be translated into colossal pseudomagnetic responses. This ability to reshape the Fermi surface and quantize electronic states purely by strain offers a versatile route to engineer novel phases without chemical substitution or external magnetic fields. Second, in the specific case of FeSn, such strain-driven Landau quantization naturally intertwines with its intrinsic kagome features—including Dirac dispersions, van Hove singularities, and flat bands—opening opportunities to explore correlated states that may be uniquely stabilized under giant pseudofields. Together, these results demonstrate that kagome lattices are not only fertile ground for

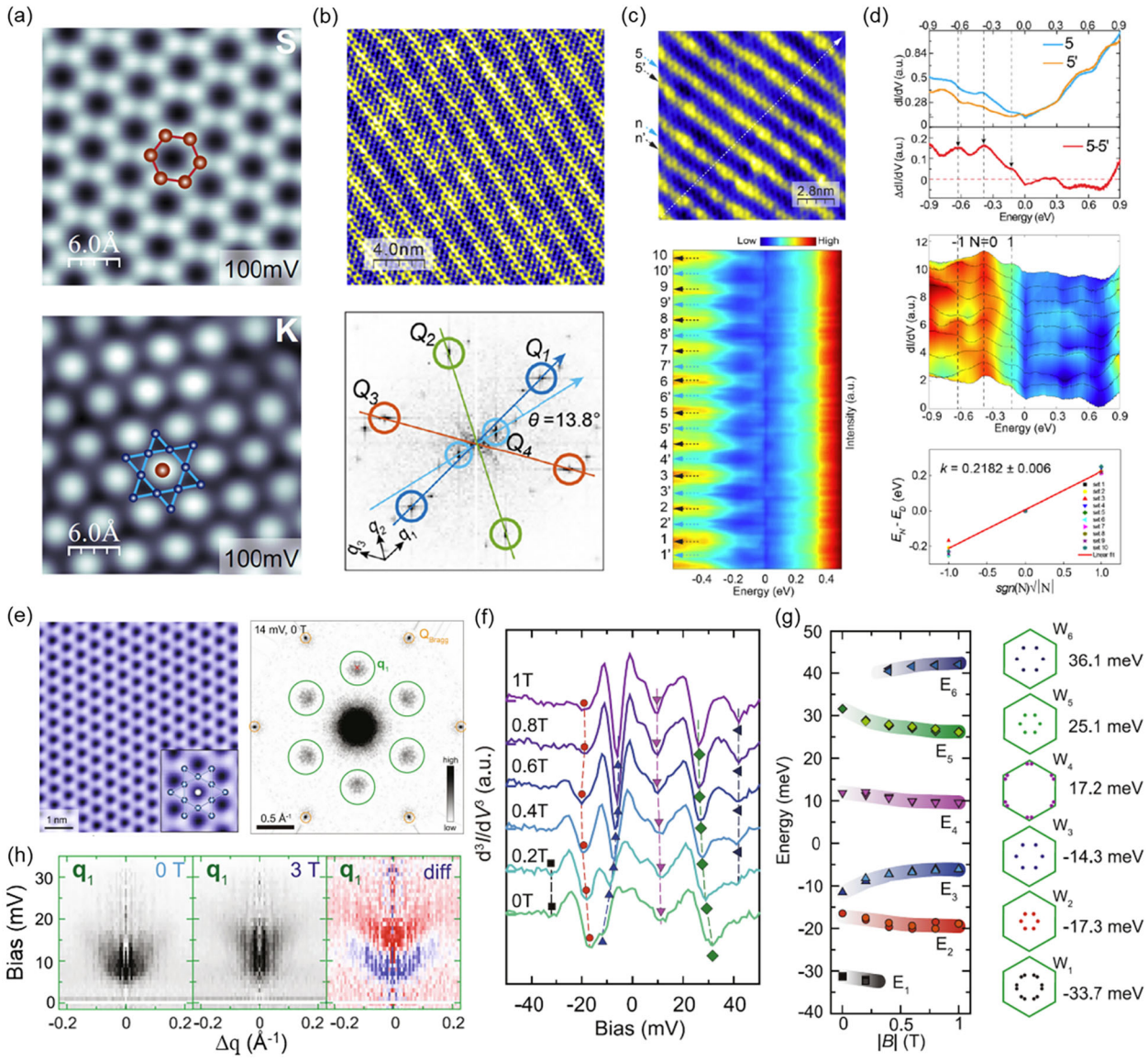

Figure 3 STM studies on kagome FeSn and Fe_3Sn_2 films. (a) Upper: Atomic resolution STM image of the S layer exhibiting a honeycomb lattice with V = 200 mV, I = 3.0 nA. Lower: Atomic resolution STM image of the K layer showing a close-packed lattice with V = 100 mV, I = 3.0 nA. (b) Left: STM topographic image of stripe modulations of Sn honeycomb lattice with V = 100 mV, I = 5.0 nA. Right: FFT of the image. Bragg peaks along three directions q_1, q_2, and q_3 are denoted by Q_1, Q_2, and Q_3 in blue, green and red circles, respectively. The diffraction peak of the stripe modulation is denoted by Q_4 in cyan circles. There is an angle of 13.8° between Q_4 and Q_1 directions. (c) Upper: STM topographic image showing the stripe modulations, where the on and between stripe sites are labeled as n′ and n, respectively. Set point: V = 1.0 V, I = 7.0 nA. Lower: dI/dV spectra taken along the white dashed arrow in the upper panel with the intensity displayed in false color. (d) Upper: dI/dV spectra taken on stripe and between strip and their difference. Middle: Difference dI/dV spectra by subtracting n and n′. The most pronounced peak at −0.36 eV is assigned to $N = 0$th Landau level and the neighboring two peaks are assigned to $N = \pm 1$st. Lower: Plot of peak energy ($E_N - E_D$) vs $\mathrm{sgn}(N)\sqrt{|N|}$. (e) Left: High-resolution STM topograph acquired at the Fe_3Sn surface with V = 100 mV, I = 100 pA. Right: Sixfold symmetrized FT of L(r,V) = (dI/dV)/(I/V) map at 14 mV. (f) Second derivative of the spectra (d^3I/dV^3) acquired in a magnetic field applied parallel to the c-axis. (g) Dispersion of spectral peaks in the magnetic field and theoretically calculated Weyl node positions for magnetization saturated along the c-axis. (h) Radially averaged linecuts of FTs of L(r,V) maps, starting at $(Q_{Bragg,1} + Q_{Bragg,2})/3$, focusing on the reciprocal space region denoted by the green circle in (e), at 0 T (left), 3 T (middle) and their difference (right). Data in (a) is adapted from Ref. [59]. Data in (b–d) is adapted from Ref. [60], Data in (e–g) is adapted from Ref. [67]

intrinsic topological and magnetic phenomena, but also highly tunable platforms where strain provides an external "knob" for driving emergent electronic behavior.

The kagome magnet Fe_3Sn_2 provides a striking example of how the interplay between magnetism and band topology can generate a wealth of emergent electronic states.

STM and spectroscopic measurements on thin films reveal a dense array of spectroscopic features straddling the Fermi level, consistent with theoretical predictions of low-energy Weyl fermions and associated Fermi arc surface states (Figs. 3(e)–(f)) [67]. The application of a magnetic field induces pronounced shifts in these features, whose energies evolve systematically with the magnetization direction (Fig. 3(g)). This field-driven evolution demonstrates how spin reorientation directly reshapes the local density of states of the Weyl band structure. Further insight comes from scattering and interference imaging: a dispersing wave vector q_1, located at $(Q_{Bragg,1} + Q_{Bragg,2})/3$ and appearing just above E_F (green circle in Fig. 3(e)), exhibits a magnetic-field-dependent spectral profile, with spectral-weight transfer clearly resolved in the numerical difference maps (Fig. 3(h)). Notably, the dispersion velocity of q_1 is far smaller than that of Dirac fermions reported by ARPES, underscoring that the observed states are unlikely to originate from Dirac dispersions.

Taken together with earlier reports of massive Dirac fermions and flat bands in Fe_3Sn_2 [22], these observations position this material as a uniquely versatile kagome platform where Weyl fermions, Fermi arcs, and correlated states coexist and can be tuned by magnetic degrees of freedom. In this sense, Fe_3Sn_2 exemplifies how kagome magnets merge topology and strong correlations, establishing them as fertile ground for discovering new electronic phases.

3.2 Symmetry breaking in kagome FeSn films

Recent STM/S studies on Fe_3Sn-terminated FeSn thin films grown on $SrTiO_3(111)$ have revealed that the kagome lattice undergoes a trimerization, breaking its six-fold rotational and mirror symmetries while preserving translational invariance [59]. This trimerized state manifests as an energy-dependent contrast reversal in dI/dV maps, with up- and down-triangle sites exchanging spectral weight across a characteristic crossing energy ($\sim$16.8 meV), and the central Sn site dominating near $\sim$100 meV [Figs. 4(a)–(b)]. Such behavior reflects an unusual redistribution of electronic density across inequivalent sublattices. Defects further amplify this broken-symmetry state. Sn vacancies, the most prevalent defect in FeSn, induce sharp in-gap bound states that strongly enhance the trimerized contrast, producing distinctive three-lobe features in dI/dV maps [Figs. 4(c)–(d)]. Interestingly, these vacancy-induced states evolve with energy: while deeper states retain approximate three-fold symmetry, those closer to the Fermi level display a pronounced two-fold anisotropy, suggestive of an emergent nematic response intertwined with the defect potential.

Beyond defects, the trimerized kagome state is highly tunable by magnetic fields. Although STM imaging employed non-spin-polarized tips, the application of an in-plane magnetic field markedly enhanced energy-dependent stripe modulations of the lattice [Figs. 4(e)–(f)]. At certain energies, the modulation locks into specific crystallographic directions, while at others it gives rise to emergent honeycomb-like patterns. Moreover, the defect-bound states themselves shift systematically with the field orientation, exhibiting a two-fold angular dependence in both the kagome and Sn layers, offset by $\sim$30°, consistent with the relative lattice rotation [Fig. 4(g)]. These observations point to a deeply entangled coupling between charge, lattice, and spin degrees of freedom in FeSn, where electronic nematicity and trimerization can be sensitively tuned by external magnetic fields.

Collectively, these results demonstrate that FeSn provides a paradigmatic platform to explore symmetry-breaking instabilities in a kagome lattice. The coexistence of trimerization, nematic modulations, and field-tunable bound states highlights the richness of correlated kagome metals, linking local defect physics to long-range electronic order and offering a versatile route to engineer quantum phases through symmetry control.

3.3 Room-temperature ferromagnetism in FeSb kagome films

Recent progress has demonstrated that epitaxial growth can stabilize non–vdW 2D ferromagnets [109], offering an alternative pathway beyond exfoliation. A notable example is bilayer FeSb grown on $SrTiO_3(001)$ [93], which represents a rare case of a 2D non–vdW ferromagnet exhibiting robust room-temperature order. STM reveals that the FeSb film conforms to the step-terrace morphology of the $SrTiO_3$ substrate (Fig. 5(a)). Thickness analysis from line profiles indicates a value of $\sim$1.0 nm, consistent with a bilayer structure (Fig. 5(b)). The surface exhibits multiple domains tens of nanometers across, reflecting the symmetry mismatch between the threefold FeSb lattice and the fourfold $SrTiO_3$ substrate. Within individual domains, atomic-resolution imaging resolves a well-defined kagome lattice (Fig. 5(c)), whose periodicity is four times the FeSb lattice constant. Line profiles (Fig. 5(d)) further reveal contrast variations of $\sim$1.2 Å between different lattice sites.

Spectroscopic characterization shows a metallic density of states with multiple features (Figs. 5(e)–(f)). Distinct peaks in the differential conductance spectra, measured at representative hexagon and triangle sites, highlight enhanced electronic weight at the shared triangle corners of the kagome lattice. Spatially resolved dI/dV maps (Fig. 5(f)) further emphasize the following behavior. At negative bias near −0.7 eV, high contrast emerges at the shared triangle sites, consistent with the presence of a flat band characteristic of kagome systems, while features closer to the Fermi level display finer structural details such as ring-like and six-lobe motifs. At positive energies, the electronic contrast shifts toward the center of the

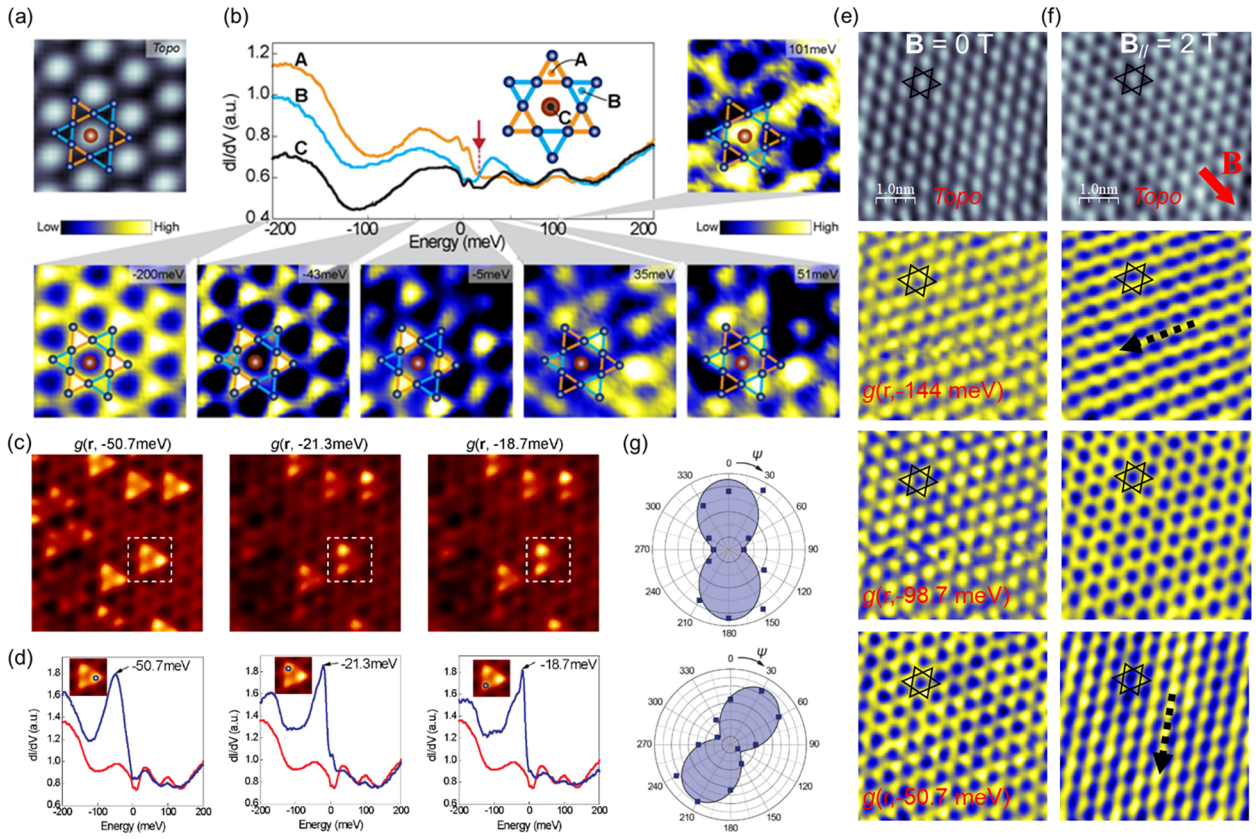

Figure 4 Symmetry breaking in kagome FeSn films. (a) Topographic STM image of the Fe_3Sn layer with V = 200 mV, I = 5.0 nA. (b) dI/dV spectra taken at three representative sites labeled A, B, and C (inset) and differential conductance maps of the same location at the energies marked. A ball-and-stick model of the kagome lattice is overlaid on the STM image and differential conductance maps. (c) dI/dV maps recorded at the bound state energies indicated. Set point: V = 200 mV, I = 5.0 nA. (d) dI/dV spectra (red) measured at one of the lobes marked by the red circles and away from the defect (black). (e) Topographic STM image and dI/dV maps at −144, −98.7, and −50.7 meV under B = 0 T with V = 200 mV, I = 0.7 nA. (f) Same as (e) but with an in-plane magnetic field $B_{//}$ = 2 T along the direction marked by the red arrow. (g) Polar plots of the angle-dependent bound states on the Sn and kagome layers, respectively. Data in (a–f) is adapted from Ref. [59]. Data in (g) is adapted from Ref. [108]

kagome hexagons. These observations are corroborated by density-functional theory calculations, underscoring the stability of a kagome surface termination in bilayer FeSb.

Magnetic measurements reinforce the significance of this system for 2D spintronics. After capping with amorphous Sb, ex situ magnetometry reveals clear hysteresis loops across a wide temperature range (Fig. 5(g)). The coercive field decreases with increasing temperature, yet the persistence of a pronounced loop at 300 K demonstrates robust ferromagnetic order above room temperature. The magnetization is strongly anisotropic, with an in-plane easy axis, distinguishing FeSb from many vdW magnets whose ordering temperatures are typically much lower.

Together, these results establish bilayer FeSb as an archetype of non–vdW 2D ferromagnets. The simultaneous realization of a kagome lattice and high-T_c ferromagnetism makes this material a compelling platform for exploring the interplay of flat-band physics, magnetism, and topology, pointing toward new opportunities in spintronic applications.

3.4 Kagome architectures revealed by STM in supramolecular assemblies and elemental adatom lattices

While naturally occurring kagome materials are scarce, recent advances in supramolecular assembly, on-surface synthesis, and epitaxial growth have enabled the controlled fabrication of artificial kagome networks with unprecedented precision, offering model systems to probe their electronic and magnetic properties [99–104, 106]. A particularly versatile approach has been the use of supramolecular self-assembly. For example, porphyrin-based building blocks have been used to generate the metal–organic coordination kagome network (Fig. 6(a)) [100]. This system is notable because the porphyrin cores can be metalated with transition metals such as Fe or

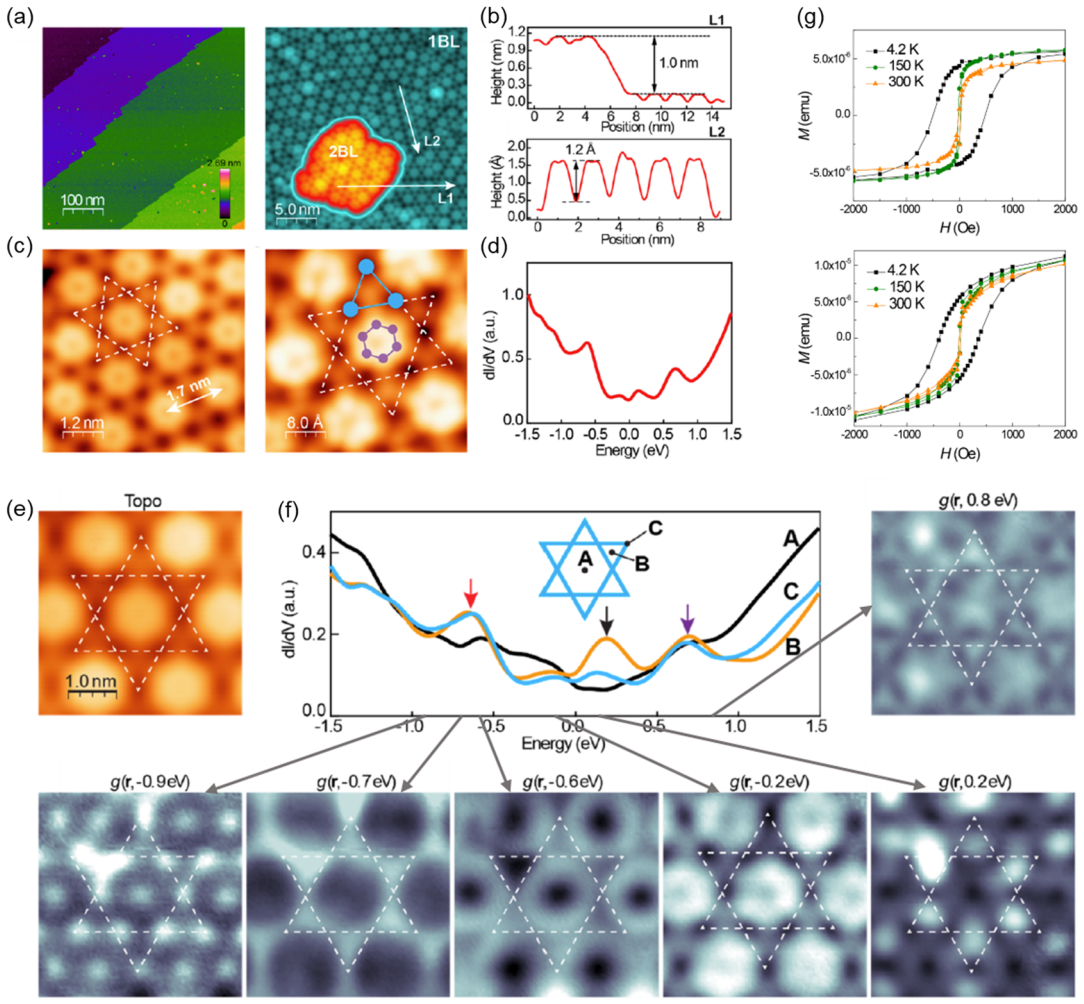

Figure 5 Room-temperature ferromagnetism in epitaxial bilayer FeSb films. (a) Left: Topographic STM image of a 1 BL FeSb film epitaxially grown on the $SrTiO_3$ substrate with V = 2.0 V, I = 10 pA. Right: Topographic STM image of a 2 BL FeSb island with V = 1.0 V, I = 50 pA. (b) Line profile along white arrow L1 and L2 in (a). The height of the 1 BL film is determined to be 1.0 nm. The high-low contrast of the surface reconstruction is 1.2 Å. (c) Left: Atomic resolution STM image of the 1 BL FeSb film showing a kagome lattice. Set point: V = –0.1 V, I = 600 pA. Right: Close-up view of the kagome lattice revealing the enhanced density of state at the center (purple hexagon) and the suppressed density of state at the shared triangle site (cyan triangle). Set point: V = 0.1 mV, I = 200 pA. (d) Typical dI/dV spectrum of the 1 BL FeSb film taken at the corner of the shared triangle site (cyan dot site in (c)). (e) Topographic STM image of the kagome lattice. Set point: V = 1.0 V, I = 1.0 nA. (f) dI/dV spectra taken at the A (center), B (center of the shared triangle), and C (corner of the shared triangle) sites and differential conductance maps at the energy specified. The red, black, and purple arrows mark the peaks at –0.66, 0.18, and 0.69 eV, respectively. (g) In-plane and out-of-plane M-H hysteresis loops under 4.2 K, 150 K and 300 K. Data in (a–g) is adapted from Ref. [93]

Co, introducing local magnetic moments and enabling bimetallic functionalities. Similarly, hydrogen-bond-driven assembly of diboraperylene diborinic acid derivatives B_2-Per on Ag(111) has led to the formation of a chiral kagome network (Fig. 6(b)), which hosts a flat band localized at the molecular centers [101]. The observation of such a band close to the Fermi level directly confirms the promise of self-assembled organic kagome lattices as tunable flat-band platforms. Expanding on this theme, hierarchical supramolecular engineering of linear dicarbonitrile polyphenyl molecules has produced a variety of tessellated kagome patterns, including previously unobserved chiral lattices with long-range order (Fig. 6(c)) [102]. Likewise, hydrogen-bonded organic frameworks on noble-metal surfaces provide a flexible means of creating electronic kagome lattices with tailored potential landscapes (Fig. 6(d)), where both regular and breathing-type lattices exhibit edge states consistent with nontrivial topology [103].

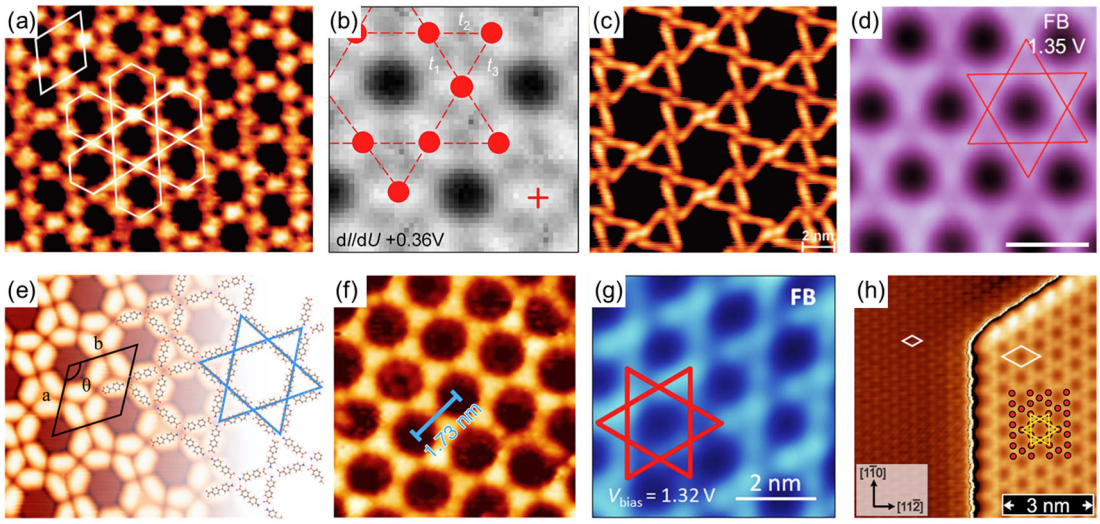

Figure 6 STM results on organic or metal kagome films on metal substrates. (a) High-resolution STM image (25 nm × 20 nm) of porphyrin/Au(111) (V = −1.3 V, I = 300 pA). The rhombic-shape frame defines the network unit cell with a constant of 4.1 nm. The network frame highlights the kagome lattice. (b) High-resolution STM image of B_2-Per/Ag(111) (V = −1 V, I = 100 pA). (c) Kagome lattice formed by NC-Ph_5-CN molecules, comprising four-fold nodes and quasi-hexagonal and trigonal cavities. (d) dI/dV maps of benzene/Br/Ag(111) obtained at energies of 1.35 eV. (e) High-resolution STM image of 4-aninobiphenyl-4′-carboxylic acid/Cu(111) surface. The rhombus gives the unit cell. (f) STM images of P^2TANG on Au(111) kept at 210 °C (V = −1.12 V, I = −0.99 nA). (g) DOS mappings at the FB on twisted multilayer silicene (V = 1.32 V, I = 100 pA). (h) Atomic resolution image of Ni/Pb(111). Red dots represent the 2D Ni kagome lattice (yellow hexagram) (V = 10 mV, I = 1.0 nA). Data in (a), (b), (c), (d), (e), (f), (g) and (h) is adapted from Ref. [100], Ref. [101], Ref. [102], Ref. [103], Ref. [106], Ref. [104], Ref. [95] and Ref. [75], respectively

Remarkably, even self-assembled hydrogen-bonded kagome structures can undergo in situ transformation into metal–organic kagome lattices while retaining chirality (Fig. 6(e)), illustrating the chemical versatility of this strategy [106]. Extending this approach to 2D conjugated polymers has recently yielded mesoscale ordered kagome lattices [Fig. 6(f)], where azatriangulene precursors combined with a hot-dosing strategy produced semiconducting networks with both Dirac cones and flat bands [104]. This breakthrough overcomes previous barriers of limited domain size and high defect density, marking an important advance toward integrating kagome polymers into electronic devices.

Beyond molecular assembly, elemental adatom systems have also provided compelling kagome realizations. In twisted multilayer silicene, moiré engineering induces a robust electronic kagome lattice (Fig. 6(g)), where quantum destructive interference quenches electron kinetic energy, giving rise to flat bands and associated edge states [95]. This platform demonstrates how structural twisting in 2D materials can drive kagome physics and potentially host fractional Chern insulating states. Similarly, a monolayer Ni kagome lattice grown on Pb(111) (Fig. 6(h)) reveals flat-band features near −0.2 eV, alongside proximity-enhanced superconductivity from the substrate, thereby offering a unique opportunity to explore the interplay between kagome flat bands and superconductivity at the atomic limit [75].

Considering all of the above, supramolecular assemblies and elemental adatom lattices offer complementary strategies for creating kagome architectures. Whereas supramolecular systems excel in chemical tunability and functionality, elemental frameworks provide unmatched atomic precision. The combined insights from these STM studies establish a versatile foundation for exploring kagome physics, from band topology to correlated electronic states, in artificially engineered materials.

Advances in layered chalcogenides have enabled the identification of a coloring-triangle lattice in ultrathin Cr_8Se_{12}, which generates kagome-like electronic bands within a semiconducting 2D transition metal chalcogenide [94]. This approach provides an avenue to engineer Kagome physics directly into semiconductors relevant for device integration. Layered Nb_3Cl_8 provides a rare platform where strong electronic correlations give rise to robust Mott insulating states persisting down to the monolayer limit. Recent studies reveal a nearly thickness-independent Mott gap, but with an unexpected parity-dependent modulation of the local density of states between odd and even layers [98]. This behavior highlights how interlayer dimerization and correlation effects intertwine to shape the ground state, underscoring the delicate balance between electronic correlation and interlayer coupling in vdW in-

sulators. This establishes Nb_3Cl_8 as a model platform for understanding Mottness and the tunability of correlated states in vdWs insulators.

4 ARPES studies: electronic structure of kagome films

ARPES has emerged as a pivotal tool for directly probing the electronic structure of kagome materials, offering insights into their unique band topology, correlation effects, and emergent quantum states [110, 111]. This section reviews recent ARPES studies on kagome films, highlighting key experimental findings and their implications for understanding Dirac cones, flat bands, and van Hove singularities in these systems.

4.1 ARPES insights into FeSn and CoSn films

Understanding the microscopic origin of magnetism in kagome systems requires distinguishing between itinerant and localized scenarios. In metallic compounds, a Stoner instability associated with a high density of states at the Fermi level drives spin splitting, which collapses above the Néel temperature (T_N) [112]. By contrast, in localized-moment systems, magnetism arises from Heisenberg exchange between persistent local moments, and exchange splitting diminishes only gradually with temperature [113]. This distinction is particularly relevant for kagome lattices, where quantum destructive interference generates flat bands. Theoretical work based on the Hubbard model applied to a half-filled flat band predicts a ferromagnetic ground state [114], aligning conceptually with the Stoner mechanism of itinerant magnetism. However, experimental evidence of the magnetic splitting across T_N has not been collected yet. This is primarily due to their characteristically high T_N, which exceed the practical limits for temperature-dependent ARPES measurements probing the required energy and momentum resolutions. Consequently, the fundamental nature of magnetism in these kagome systems—whether dominantly itinerant or localized—remains an unresolved and actively debated question.

Epitaxial kagome FeSn films have recently emerged as an ideal platform to overcome this limitation [56–63]. Building upon earlier synchrotron-based ARPES studies of FeSn bulk crystals that identified Dirac cones and flat band signatures [24, 115], thin films with improved surface quality allow long-term, thermally stable mapping from cryogenic to elevated temperatures [63]. Fermi-surface maps reveal the characteristic flower-like contours at $\overline{\Gamma}$, accompanied by flat-band signatures near −1.2 eV (Figs. 7(a)–(b)) and Dirac cones at $\overline{K}$ with a Dirac point around −0.35 eV (Fig. 7(c)). Temperature-dependent measurements show systematic band shifts along high-symmetry directions (Fig. 7(d)), which persist well above T_N and cannot be explained by lattice expansion. Such robustness cannot be explained by trivial thermal expansion alone. Instead, the persistence of splitting in the paramagnetic state points to a strong localized-moment component in FeSn magnetism, highlighting the dual itinerant–localized character of kagome magnetism.

Equally revealing is the orbital dependence of electronic correlations. Detailed analysis shows that the flower-like electron bands at $\overline{\Gamma}$, derived from the d_{xy} + $d_{x^2-y^2}$ spin-majority orbitals, are heavily renormalized with an effective mass $m^* = 7\, m_e$ (Fig. 7(e)). In contrast, the Dirac cones at $\overline{K}$ and hole-like bands at $\overline{\Gamma}$ remain weakly renormalized. This orbital-selective renormalization indicates that electron correlations in FeSn act very unevenly across different orbital sectors, a phenomenon reminiscent of multiorbital physics in iron-based superconductors [116, 117] and ruthenates [118, 119]. These results suggest that kagome systems may host a similar landscape of selective correlation strength, with flat bands being particularly susceptible to strong renormalization.

Parallel studies on CoSn thin films have revealed complementary insights [68]. ARPES measurements identify two nearly dispersionless bands: FB1, located close to the Fermi level, and FB2, at deeper binding energies (Fig. 7(f)). FB1 is characterized by an exceptionally large effective mass ($m^* = 16.7\, m_e$), underscoring its flat-band nature and making it highly sensitive to doping or gating. Indeed, theory predicts that a modest upward shift of FB1 could drive the system into a low-temperature antiferromagnetic phase, suggesting that electronic filling control may unlock hidden ordered states. More strikingly, ARPES directly resolves spin-orbit-coupling gaps where FB2 intersects quadratic dispersions, with gap magnitudes of 0.09–0.12 eV (Fig. 7(g)). These values are significantly larger than those previously reported in bulk CoSn [50, 51], underscoring the advantages of thin-film platforms for enhancing intrinsic topological features. The coexistence of nearly flat bands with large spin-orbit-coupling gaps provides compelling evidences for topologically nontrivial flat bands in kagome systems.

Overall, these advances establish FeSn and CoSn films as model systems for disentangling the interplay of itinerant and localized magnetism, orbital-selective correlation, and flat-band topology in kagome metals. They demonstrate that thin-film ARPES can not only overcome limitations of bulk crystals but also reveal emergent many-body phenomena—paving the way for tuning kagome-derived states toward magnetism and topological phases.

4.2 ARPES investigations of engineered kagome films on Si(111) and Au(111)

Progress in kagome physics has been closely tied to advances in materials synthesis, where the challenges lie in producing high-quality 2D lattices that preserve the flat-band character of kagome electronic structures. Epitaxial

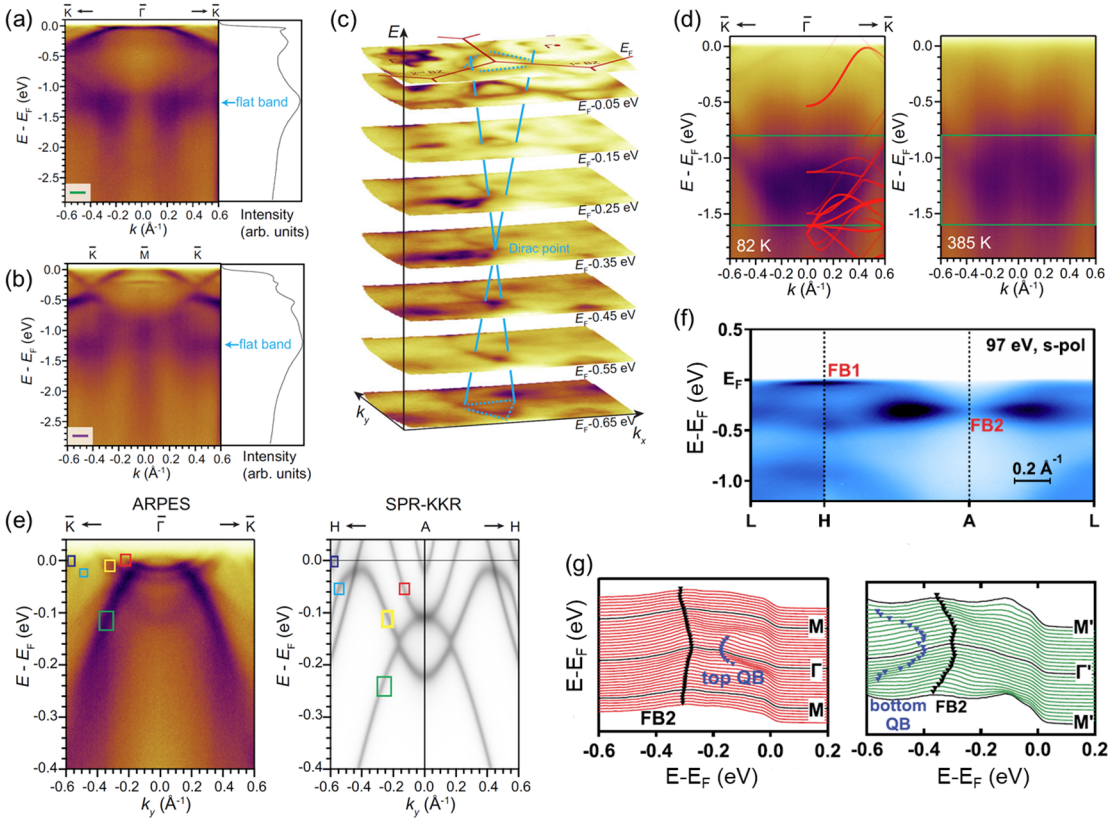

Figure 7 Band renormalization, flat band splitting and topological nature in FeSn and CoSn films. (a) $\overline{\mathrm{K}}-\overline{\Gamma}-\overline{\mathrm{K}}$ cuts of FeSn films taken at 83 K and their momentum-integrated EDCs. (b) Same as (a) but for cut along $\overline{\mathrm{K}}-\overline{\mathrm{M}}-\overline{\mathrm{K}}$. (c) Constant energy contours. Blue solid and dashed lines denote the Dirac dispersions. (d) Left: $\overline{\mathrm{K}}-\overline{\Gamma}-\overline{\mathrm{K}}$ cuts taken at 82 K. Spin majority-projected density-functional theory calculations are superimposed on the cut. Right: $\overline{\mathrm{K}}-\overline{\Gamma}-\overline{\mathrm{K}}$ cuts taken at 385 K. (e) Comparison of the $\overline{\mathrm{K}}-\overline{\Gamma}-\overline{\mathrm{K}}$ cut in ARPES data and SPR-KKR calculations. (f) ARPES spectra in the $k_z = \pi$ plane of CoSn films, measured with 97 eV s-polarized photons. (g) EDCs stack along the $\mathrm{M}-\Gamma-\mathrm{M}$ and $\mathrm{M}'-\Gamma'-\mathrm{M}'$ directions. The black and blue delta symbols mark the position of peaks from FB2 and the top QB, respectively. Data in (a–e) and (f–g) is adapted from Ref. [63] and Ref. [68], respectively

growth on functional substrates has recently emerged as a powerful route, with ARPES providing direct access to the resulting band dispersions. In this context, semiconducting substrates such as Si(111) are particularly attractive: their surface reconstructions offer natural 2D templates, the substrate band gap minimizes interference near the Fermi level, and the wide choice of deposition elements enables flexible tuning of lattice and electronic properties [120].

A notable example is the Ag/Si(111) system, which hosts a distorted breathing kagome lattice. ARPES measurements reveal the key ingredients of kagome physics: a nearly flat band, dispersive states derived from hybridized d-orbitals, and quadratic band touching near the zone center (Figs. 8(a)–(b)) [77]. Analysis indicates that these bands originate predominantly from the topmost Ag and Si layers, in agreement with density functional theory. Tight-binding calculations further confirm that all three bands derive from the Ag kagome lattice. Although the small spin–orbit coupling of Ag limits the gap opening the quadratic band and the flat band, theory suggests that substituting heavier elements could stabilize topological flat bands, providing a promising direction for future design.

Beyond Ag/Si(111), rare-earth-based kagome compounds offer an additional route to engineer band filling and electronic topology. In particular, the $GdPb_3$/Si(111) and $YbPb_3$/Si(111) systems display nearly identical kagome-derived band structures due to their similar atomic arrangements, yet their Fermi levels differ substantially as a result of the distinct valence configurations of Gd and Yb (Fig. 8(c)) [74]. This shift, on the order of ~0.5 eV, reflects charge transfer from the Pb layer required to maintain bonding, and enables controlled tuning of the electronic structure in mixed phases such as $Gd_xYb_{1-x}Pb_3$. ARPES spectra confirm that increasing Yb concentration continuously lowers the Fermi level relative to the Si bands. A key consequence is the emergence of a Lifshitz transition, as the Fermi level moves from just above to intersecting the kagome-derived band structure. This induces a qualitative change in the Fermi surface topology:

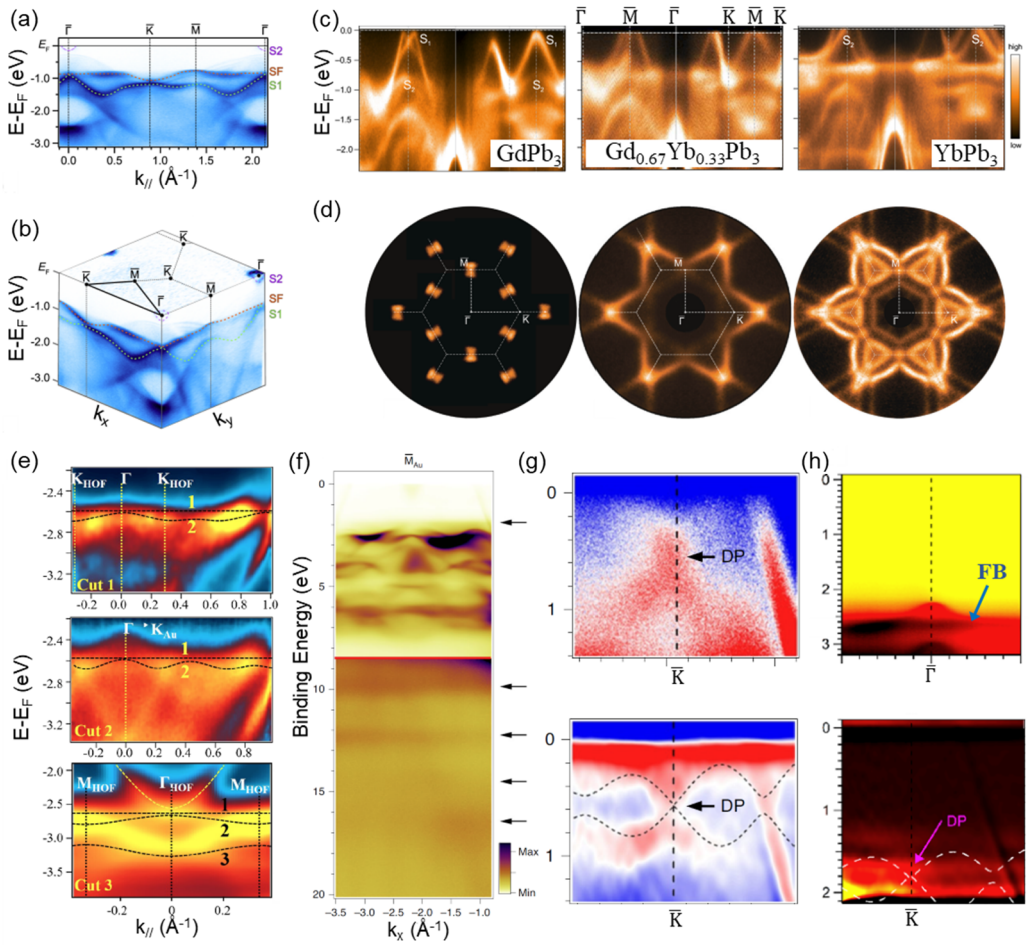

Figure 8 Flat band and Dirac cones in kagome films on Si(111) and Au(111). (a) ARPES spectra of the Ag/Si(111) along the $\overline{\Gamma}-\overline{K}-\overline{M}-\overline{\Gamma}$ path. (b) 3D ARPES plot of the Ag/Si(111). The dotted gray lines represent the BZs with high-symmetry points denoted. The topmost surface represents the E_F. The three surface bands (S1, SF, and S2) are highlighted by green, orange, and purple dotted lines, respectively. (c) Experimental ARPES spectra measured at 78 K for $GdPb_3$/Si(111), $Gd_{0.67}Yb_{0.33}Pb_3$/Si(111) and $YbPb_3$/Si(111). (d) Fermi surfaces of $GdPb_3$/Si(111), $Gd_{0.67}Yb_{0.33}Pb_3$/Si(111) and $YbPb_3$/Si(111). (e) High-resolution ARPES of THPB/Au(111) measured at 12 K along the Γ-K_{HOF}, Γ-K_{Au} and M_{HOF}-Γ_{HOF}-M_{HOF} directions. K_{HOF}, Γ_{HOF} and M_{HOF} are special k points in the BZ of THPB HOF. (f) ARPES data for P^2TANG/Au(111) measured with photon energies of 30 eV. The ARPES signal from the 8–20 eV region (below the red line) has been multiplied by a factor of 12 to highlight the experimental P^2TANG flat states, marked by black arrows. (g) ARPES signal from P^2TANG/Au(111) at 30 eV and The corresponding second-derivative maps. The dashed lines represent calculated bands for free-standing P2TANG. The label DP and black arrow highlight the Dirac point location. (h) ARPES spectra of P^2TANGO on Au(111) around the $\overline{\Gamma}$ and $\overline{K}$ points. Data in (a–b), (c–d), (e), (f–g) and (h) is adapted from Ref. [77], Ref. [74], Ref. [121], Ref. [104] and Ref. [99], respectively

pure $GdPb_3$/Si(111) exhibits six small hole pockets near the $\overline{M}$ points, whereas in $Gd_{0.67}Yb_{0.33}Pb_3$/Si(111) these evolve into a large contour around $\overline{\Gamma}$ accompanied by additional features at $\overline{M}$ and $\overline{K}$ (Fig. 8(d)). Such topology changes, driven by modest adjustments in band filling, are expected to strongly influence physical properties, highlighting rare-earth kagome heterostructures as a versatile platform for studying Fermi-surface instabilities.

Organic kagome frameworks grown on metal surfaces open a complementary avenue for realizing flat-band physics through bottom-up molecular design. A striking example is the self-assembly of monolayer of 2D hydrogen-bond organic frameworks (HOFs) of 1,3,5-tris(4-hydroxyphenyl)benzene (THPB) on Au(111) substrate, which form large, single-orientation domains suitable for spectroscopic investigation [121]. ARPES reveals the presence of a flat band across the entire Brillouin zone, consistent with theoretical expectations, despite partial overlap with the Au surface state (Fig. 8(e)). These results demonstrate that self-assembly of organic molecules can stabilize extended kagome lattices with well-defined band structures, an advance that significantly expands the materials base for flat-band studies beyond inorganic solids.

Equally compelling progress has been achieved in π-conjugated kagome polymers, where extended electronic conjugation offers a natural route to Dirac cones and flat bands [99, 104]. Mesoscale-ordered P^2TANG lattices on Au(111) provide sufficient coherence for ARPES characterization, revealing a prominent flat band 1.8 eV below the Fermi level together with polymer-derived dispersions that match closely with density functional theory (Figs. 8(f)–(g)) [104]. Related derivatives such as P^2TANGO further confirm the coexistence of flat bands and Dirac cones, although with notable shifts in the Dirac point energy due to changes in bridging functionality (Fig. 8(h)) [99]. This chemical tunability directly links molecular design to electronic topology, allowing systematic exploration of kagome-derived quantum states.

These collective investigations establish substrate engineering as a transformative paradigm. Semiconductor templates provide ideal platforms for isolating and chemically tuning inorganic kagome states, while metal surfaces facilitate organic self-assembly pathways toward designer topological band structures. ARPES validates both approaches as complementary routes to realizing correlated electron phenomena in tailored quantum materials, significantly expanding the experimental frontier for exploring flat band physics beyond conventional solid-state systems. The demonstrated precision in controlling band topology through atomic-scale design provides new opportunities for discovering emergent quantum states in frustrated lattice architectures.

5 Outlook and perspectives

The exceptional electronic and magnetic properties of kagome thin films, rooted in geometric frustration and quantum confinement effects, make them ideal candidates for potential applications in quantum computing and spintronics. This part will focus on the significance of kagome thin films, challenges in high-quality kagome thin film preparation, and perspectives on the 2D thickness limit to clarify novel band structures such as flat bands and Dirac cones from the bulk bands.

5.1 Significance of kagome thin films

Kagome thin films, due to their inherence of the unique electronic and magnetic properties of the kagome lattice, hold great promise for a wide range of applications in emerging technologies, such as quantum computing and spin-based electronics. On the one hand, the flat bands of the kagome lattice introduce the emergence of strongly correlated electron states, which are essential for the realization of quantum qubits. The high density of states induced by flat bands enhances the electron interaction and allows the creation of qubits with long coherence times, which enables qubits operating at higher temperatures and with greater stability compared to existing qubit technologies. On the other hand, the topological states are less sensitive to external perturbations such as impurities and thermal fluctuations, and thus the topological protection of certain quantum states can provide a robust platform for quantum information processing. Moreover, the geometric frustration in the kagome lattice lead to spin-liquid-like behaviors, where spins remain in a dynamic, fluctuating state even at absolute zero temperature, instead of forming a static, ordered pattern like in a typical magnet. These spin-liquid states can potentially be exploited for developing high-density magnetic storage devices with enhanced stability and low power consumption compared to traditional ferromagnetic materials. Additionally, the large magnetic anisotropy and the presence of topological magnetic states in kagome thin film materials can be utilized to create spin-filters and spin-valves, which are crucial components for high speed and low power consumption data processing in future spin-based electronics.

5.2 Challenges in high-quality kagome thin film preparation

High-quality thin film growth lays the groundwork for the development and production of advanced devices. The challenges to prepare high quality kagome thin films mainly exist in issues including complex multi-element composition, non-layer structure and lattice mismatch between the film and substrate. The multi-component nature of many kagome-lattice-based materials poses significant difficulties in achieving precise control over the stoichiometry and distribution of elements during the growth process. Any deviation from the optimal stoichiometry can lead to the formation of inhomogeneity, defects with a degradation of the desired physical properties, and even different phases. The non-layer structure, such as binary kagome compounds T_mX_n makes it difficult to ensure the uniform growth of the lattice across the substrate, and leads to the formation of defects such as dislocations, vacancies, and grain boundaries, which significantly impact on the electrical and magnetic properties of the kagome thin films. Additionally, lattice mismatch between the substrate and the kagome film usually generates compressive or tensile stress within the film, which distort the atomic arrangement within the film, leading to defects such as cracks and dislocations, and further affecting the film's electrical and magnetic properties. Moreover, the interfacial effect usually strongly correlated with the thickness of the epitaxial film, which gives hints about the interplay of the substrate.

Currently, the growth techniques available for kagome thin films are limited to MBE and magnetron sputtering. One of the key advantages of MBE is its ability to achieve atomic-level precision in controlling the film's composition, doping as well as thickness. The practice of MBE also allows for the construction of high-quality interfaces between kagome films and functional layers, crucial for

applications such as spin-electronics, where the quality of the material interfaces determines the spin-transport properties. However, the low growth rates and expensive cost make large-scale industrial production of kagome thin films tough. Thus, it is necessary to develop new techniques with the advantages of low cost and rapid fabrication, integrated with conventional semiconductor devices to explore their application in novel electronic devices. Also, to seek alternative kagome film materials with similar performance but lower cost and easier preparation is highly required. In this respect, materials genomics, combined with theoretical calculations and high-throughput experiments, which can rapidly screen and design kagome materials may be one of the solutions.

5.3 Perspective on the kagome thin films in two-dimensional limit

The pursuit of well-defined flat band and Dirac cone band structures has long been a core focus in condensed matter physics, as these unique electronic states enable exotic quantum phenomena and high-performance device functionalities. Reducing materials to the 2D limit has emerged as a powerful strategy to optimize band clarity. First, the 2D confinement provides unique route to modulates the electronic band dispersions. The 2D confinement drastically reduces the dimensionality of the electron gas, constraining electron motion to a quasi-2D space, which in principle suppresses interlayer electron hopping, narrows the bandwidth of targeted energy bands, and ultimately stabilizes sharp, non-dispersive flat bands. The 2D restriction also reinforces the linear energy-momentum relationship of Dirac cone structure and minimize the influence of out-of-plane perturbations that often blur their characteristic conical shape in bulk materials. Second, thin films down to a few atomic layers offer exceptional control over structural defects, interface quality and strain inhomogeneities, which are key to obtain intrinsic and sharp band structures. Last but not the least, the reduced dimensionality of 2D thin films enhances the responsiveness to external tuning such as electrostatic gating, magnetic fields, or dielectric encapsulation, allowing for fine adjustment of the Fermi level relative to flat bands, enabling the manipulation of correlated electron effects.

To summarize, kagome thin films in 2D limit leverage dimensionality-induced band modulation, structural precision, and enhanced external tunability to overcome the limitations of bulk materials. This approach not only hold great promises to clarify clear flat band and Dirac cone band structures but also paves the way for their practical application in quantum computing, spintronics, and topological devices.

Supplementary information

Supplementary information accompanies this paper at https://doi.org/10.1007/s44214-025-00098-0.

Additional file 1. RightsLink Printable License (ZIP 9.6 MB)

Author contributions

YQC and HMZ wrote the draft of this manuscript; VVU and JJZ revised and provided suggestions to the manuscript. All the authors read, revised, and approved the final version.

Funding information

We acknowledge support from the National Key Research and Development Program of China (2023YFB3809600, 2024YFE0213500), National Natural Science Foundation of China (Grant No. T2495211, 12304210), Young Top Talents in "Xingliao Talent Program" of Liaoning Province (XLYC2403120), Natural Science Foundation of Liaoning Province (2023-BSBA-085), Fundamental Research Funds for the Central Universities (DUT24RC(3)015, DUT24RC(3)039).

Data availability

The data that support the findings of this study are available from the corresponding author upon reasonable request.

Declarations

Competing interests

The authors declare no competing interests.

Author details

[1]Key Laboratory of Materials Modification by Laser, Ion and Electron Beams (Dalian University of Technology), Ministry of Education, School of Physics, Dalian 116024, China. [2]Department of Physics, Dalian University of Technology, Dalian 116024, China. [3]DUT-BSU Joint Institute, Dalian University of Technology, Dalian 116024, China. [4]Department of Solid State Physics and Nanotechnology, Belarusian State University, Minsk 220030, Belarus. [5]Guangdong Basic Research Center of Excellence for Structure and Fundamental Interactions of Matter, Guangdong Provincial Key Laboratory of Quantum Engineering and Quantum Materials, School of Physics, South China Normal University, Guangzhou 510006, China. [6]School of Physics, South China Normal University, Guangzhou 510631, China.

Received: 24 October 2025 Revised: 11 December 2025
Accepted: 23 December 2025 Published online: 27 January 2026

References

1. J.X. Yin, B. Lian, M.Z. Hasan, Topological kagome magnets and superconductors. Nature **612**(7941), 647–657 (2022)
2. Y. Wang, H. Wu, G.T. McCandless, J.Y. Chan, M.N. Ali, Quantum states and intertwining phases in kagome materials. Nat. Rev. Phys. **5**(11), 635–658 (2023)
3. Q. Wang, H. Lei, Y. Qi, C. Felser, Topological quantum materials with kagome lattice. Acc. Mater. Res. **5**(7), 786–796 (2024)
4. Z. Zhang, J. Dai, C. Wang, H. Zhu, F. Pang, Z. Cheng, W. Ji, 2D kagome materials: theoretical insights, experimental realizations, and electronic structures. Adv. Funct. Mater. **35**(12), 2416508 (2025)
5. H.M. Guo, M. Franz, Topological insulator on the kagome lattice. Phys. Rev. B **80**(11), 113102 (2009)
6. S.-L. Yu, J.-X. Li, Chiral superconducting phase and chiral spin-density-wave phase in a Hubbard model on the kagome lattice. Phys. Rev. B **85**(14), 144402 (2012)
7. M.L. Kiesel, C. Platt, R. Thomale, Unconventional Fermi surface instabilities in the kagome Hubbard model. Phys. Rev. Lett. **110**(12), 126405 (2013)
8. W.-S. Wang, Z.-Z. Li, Y.-Y. Xiang, Q.-H. Wang, Competing electronic orders on kagome lattices at van Hove filling. Phys. Rev. B **87**(11), 115135 (2013)
9. Z. Li, J. Zhuang, L. Wang, H. Feng, Q. Gao, X. Xu, W. Hao, X. Wang, C. Zhang, K. Wu, Realization of flat band with possible nontrivial topology in electronic kagome lattice. Sci. Adv. **4**(11), eaau4511 (2018)
10. E. Tang, J.-W. Mei, X.-G. Wen, High-temperature fractional quantum Hall states. Phys. Rev. Lett. **106**(23), 236802 (2011)

11. T. Neupert, L. Santos, C. Chamon, C. Mudry, Fractional quantum Hall states at zero magnetic field. Phys. Rev. Lett. **106**(23), 236804 (2011)
12. K. Sun, H. Yao, E. Fradkin, S. Kivelson, Topological insulators and nematic phases from spontaneous symmetry breaking in 2D Fermi systems with a quadratic band crossing. Phys. Rev. Lett. **103**(4), 046811 (2009)
13. W. Zhu, S.-S. Gong, T.-S. Zeng, L. Fu, D.N. Sheng, Interaction-driven spontaneous quantum Hall effect on a kagome lattice. Phys. Rev. Lett. **117**(9), 096402 (2016)
14. A. Tanaka, H. Ueda, Stability of ferromagnetism in the Hubbard model on the kagome lattice. Phys. Rev. Lett. **90**(6), 067204 (2003)
15. Y. Chen, S. Xu, Y. Xie, C. Zhong, C. Wu, S.B. Zhang, Ferromagnetism and Wigner crystallization in kagome graphene and related structures. Phys. Rev. B **98**(3), 035135 (2018)
16. C. Wu, D. Bergman, L. Balents, S. Das Sarma, Flat bands and Wigner crystallization in the honeycomb optical lattice. Phys. Rev. Lett. **99**(7), 070401 (2007)
17. M.L. Kiesel, C. Platt, R. Thomale, Unconventional Fermi surface instabilities in the kagome Hubbard model. Phys. Rev. Lett. **110**(12), 126405 (2013)
18. M. Kang, S. Fang, J.-K. Kim, B.R. Ortiz, S.H. Ryu, J. Kim, J. Yoo, G. Sangiovanni, D. Di Sante, B.-G. Park, C. Jozwiak, A. Bostwick, E. Rotenberg, E. Kaxiras, S.D. Wilson, J.-H. Park, R. Comin, Twofold van Hove singularity and origin of charge order in topological kagome superconductor CsV_3Sb_5. Nat. Phys. **18**(3), 301–308 (2022)
19. J.-X. Yin, W. Ma, T.A. Cochran, X. Xu, S. Zhang, T.-J. Tien, N. Shumiya, G. Cheng, K. Jiang, B. Lian, Z. Song, G. Chang, I. Belopolski, D. Multer, M. Litskevich, Z.-J. Cheng, X.P. Yang, B. Swidler, H. Zhou, H. Lin, T. Neupert, Z. Wang, N. Yao, T.-R. Chang, S. Jia, M.Z. Hasan, Quantum-limit Chern topological magnetism in $TbMn_6Sn_6$. Nature **583**(7817), 533 (2020)
20. D.F. Liu, A.J. Liang, E.K. Liu, Q.N. Xu, Y.W. Li, C. Chen, D. Pei, W.J. Shi, S.K. Mo, P. Dudin, T. Kim, C. Cacho, G. Li, Y. Sun, L.X. Yang, Z.K. Liu, S.S.P. Parkin, C. Felser, Y.L. Chen, Magnetic Weyl semimetal phase in a kagome crystal. Science **365**(6459), 1282 (2019)
21. N. Morali, R. Batabyal, P.K. Nag, E. Liu, Q. Xu, Y. Sun, B. Yan, C. Felser, N. Avraham, H. Beidenkopf, Fermi-arc diversity on surface terminations of the magnetic Weyl semimetal $Co_3Sn_2S_2$. Science **365**(6459), 1286–1291 (2019)
22. L. Ye, M. Kang, J. Liu, F. von Cube, C.R. Wicker, T. Suzuki, C. Jozwiak, A. Bostwick, E. Rotenberg, D.C. Bell, L. Fu, R. Comin, J.G. Checkelsky, Massive Dirac fermions in a ferromagnetic kagome metal. Nature **555**(7698), 638 (2018)
23. Z. Hou, W. Ren, B. Ding, G. Xu, Y. Wang, B. Yang, Q. Zhang, Y. Zhang, E. Liu, F. Xu, Observation of various and spontaneous magnetic skyrmionic bubbles at room temperature in a frustrated kagome magnet with uniaxial magnetic anisotropy. Adv. Mater. **29**(29), 1701144 (2017)
24. M. Kang, L. Ye, S. Fang, J.-S. You, A. Levitan, M. Han, J.I. Facio, C. Jozwiak, A. Bostwick, E. Rotenberg, M.K. Chan, R.D. McDonald, D. Graf, K. Kaznatcheev, E. Vescovo, D.C. Bell, E. Kaxiras, J. Van den Brink, M. Richter, G.M. Prasad, J.G. Checkelsky, R. Comin, Dirac fermions and flat bands in the ideal kagome metal FeSn. Nat. Mater. **19**(2), 163 (2020)
25. X. Teng, L. Chen, F. Ye, E. Rosenberg, Z. Liu, J.X. Yin, Y.X. Jiang, J.S. Oh, M.Z. Hasan, K.J. Neubauer, B. Gao, Y. Xie, M. Hashimoto, D. Lu, C. Jozwiak, A. Bostwick, E. Rotenberg, R.J. Birgeneau, J.H. Chu, M. Yi, P. Dai, Discovery of charge density wave in a kagome lattice antiferromagnet. Nature **609**(7927), 490–495 (2022)
26. X. Teng, J.S. Oh, H. Tan, L. Chen, J. Huang, B. Gao, J.-X. Yin, J.-H. Chu, M. Hashimoto, D. Lu, C. Jozwiak, A. Bostwick, E. Rotenberg, G.E. Granroth, B. Yan, R.J. Birgeneau, P. Dai, M. Yi, Magnetism and charge density wave order in kagome FeGe. Nat. Phys. **19**(6), 814–822 (2023)
27. J.X. Yin, Y.X. Jiang, X. Teng, M.S. Hossain, S. Mardanya, T.R. Chang, Z. Ye, G. Xu, M.M. Denner, T. Neupert, B. Lienhard, H.B. Deng, C. Setty, Q. Si, G. Chang, Z. Guguchia, B. Gao, N. Shumiya, Q. Zhang, T.A. Cochran, D. Multer, M. Yi, P. Dai, M.Z. Hasan, Discovery of charge order and corresponding edge state in kagome magnet FeGe. Phys. Rev. Lett. **129**(16), 166401 (2022)
28. S. Nakatsuji, N. Kiyohara, T. Higo, Large anomalous Hall effect in a non-collinear antiferromagnet at room temperature. Nature **527**(7577), 212–215 (2015)
29. J.W. Cable, N. Wakabayashi, P. Radhakrishna, Magnetic excitations in the triangular antiferromagnets Mn_3Sn and Mn_3Ge. Phys. Rev. B **48**(9), 6159–6166 (1993)
30. B.R. Ortiz, S.M.L. Teicher, Y. Hu, J.L. Zuo, P.M. Sarte, E.C. Schueller, A.M.M. Abeykoon, M.J. Krogstad, S. Rosenkranz, R. Osborn, R. Seshadri, L. Balents, J. He, S.D. Wilson, CsV_3Sb_5: a Z_2 topological kagome metal with a superconducting ground state. Phys. Rev. Lett. **125**(24), 247002 (2020)
31. B.R. Ortiz, P.M. Sarte, E.M. Kenney, M.J. Graf, S.M.L. Teicher, R. Seshadri, S.D. Wilson, Superconductivity in the Z2 kagome metal KV_3Sb_5. Phys. Rev. Mater. **5**(3), 034801 (2021)
32. Q. Yin, Z. Tu, C. Gong, Y. Fu, S. Yan, H. Lei, Superconductivity and normal-state properties of kagome metal RbV_3Sb_5 single crystals. Chin. Phys. Lett. **38**(3), 037403 (2021)
33. S.Y. Yang, Y. Wang, B.R. Ortiz, D. Liu, J. Gayles, E. Derunova, R. Gonzalez-Hernandez, L. Smejkal, Y. Chen, S.S.P. Parkin, S.D. Wilson, E.S. Toberer, T. McQueen, M.N. Ali, Giant unconventional anomalous Hall effect in the metallic frustrated magnet candidate, KV_3Sb_5. Sci. Adv. **6**(31), eabb6003 (2020)
34. F.H. Yu, T. Wu, Z.Y. Wang, B. Lei, W.Z. Zhuo, J.J. Ying, X.H. Chen, Concurrence of anomalous Hall effect and charge density wave in a superconducting topological kagome metal. Phys. Rev. B **104**(4), L041103 (2021)
35. H. Chen, H. Yang, B. Hu, Z. Zhao, J. Yuan, Y. Xing, G. Qian, Z. Huang, G. Li, Y. Ye, S. Ma, S. Ni, H. Zhang, Q. Yin, C. Gong, Z. Tu, H. Lei, H. Tan, S. Zhou, C. Shen, X. Dong, B. Yan, Z. Wang, H.J. Gao, Roton pair density wave in a strong-coupling kagome superconductor. Nature **599**(7884), 222–228 (2021)
36. Y.X. Jiang, J.X. Yin, M.M. Denner, N. Shumiya, B.R. Ortiz, G. Xu, Z. Guguchia, J. He, M.S. Hossain, X. Liu, J. Ruff, L. Kautzsch, S.S. Zhang, G. Chang, I. Belopolski, Q. Zhang, T.A. Cochran, D. Multer, M. Litskevich, Z.J. Cheng, X.P. Yang, Z. Wang, R. Thomale, T. Neupert, S.D. Wilson, M.Z. Hasan, Unconventional chiral charge order in kagome superconductor KV_3Sb_5. Nat. Mater. **20**(10), 1353–1357 (2021)
37. L. Nie, K. Sun, W. Ma, D. Song, L. Zheng, Z. Liang, P. Wu, F. Yu, J. Li, M. Shan, D. Zhao, S. Li, B. Kang, Z. Wu, Y. Zhou, K. Liu, Z. Xiang, J. Ying, Z. Wang, T. Wu, X. Chen, Charge-density-wave-driven electronic nematicity in a kagome superconductor. Nature **604**(7904), 59–64 (2022)
38. Y. Xiang, Q. Li, Y. Li, W. Xie, H. Yang, Z. Wang, Y. Yao, H.H. Wen, Twofold symmetry of c-axis resistivity in topological kagome superconductor CsV_3Sb_5 with in-plane rotating magnetic field. Nat. Commun. **12**(1), 6727 (2021)
39. Y.S. Xu, Z.L. Ni, Y.Z. Liu, B.R. Ortiz, Q.W. Deng, S.D. Wilson, B.H. Yan, L. Balents, L. Wu, Three-state nematicity and magneto-optical Kerr effect in the charge density waves in kagome superconductors. Nat. Phys. **18**(12), 1470–1475 (2022)
40. L. Yu, C. Wang, Y. Zhang, M. Sander, S. Ni, Z. Lu, S. Ma, Z. Wang, Z. Zhao, H. Chen, K. Jiang, Y. Zhang, H. Yang, F. Zhou, X. Dong, S.L. Johnson, M.J. Graf, J. Hu, H.-J. Gao, Z. Zhao, Evidence of a hidden flux phase in the topological kagome metal CsV_3Sb_5. arXiv e-prints (2021). arXiv:2107.10714
41. C. Mielke 3rd, D. Das, J.X. Yin, H. Liu, R. Gupta, Y.X. Jiang, M. Medarde, X. Wu, H.C. Lei, J. Chang, P. Dai, Q. Si, H. Miao, R. Thomale, T. Neupert, Y. Shi, R. Khasanov, M.Z. Hasan, H. Luetkens, Z. Guguchia, Time-reversal symmetry-breaking charge order in a kagome superconductor. Nature **602**(7896), 245–250 (2022)
42. Paul Scherrer Institute, Unconventional superconductivity found in kagome metal (2023). https://www.psi.ch/en/news/science-features/unconventional-superconductivity-found-in-kagome-metal (accessed 20 Aug 2025)
43. Brookhaven National Laboratory Newsroom, First Direct Visualization of a Zero-Field Pair Density Wave (2023). https://www.bnl.gov/newsroom/news.php?a=121336 (accessed 20 Aug 2025)
44. University of Science and Technology of China (USTC) News, Important progress in kagome-superconductor research (2022). https://news.ustc.edu.cn/info/1055/78364.htm (accessed 20 Aug 2025)
45. X. Feng, K. Jiang, Z. Wang, J. Hu, Chiral flux phase in the kagome superconductor AV3Sb5. Sci. Bull. **66**(14), 1384–1388 (2021)
46. Z. Sun, H. Zhou, C. Wang, S. Kumar, D. Geng, S. Yue, H. Han, Y. Haraguchi, K. Shimada, P. Cheng, L. Chen, Y. Shi, K. Wu, S. Meng, B. Feng, Observation of topological flat bands in the kagome semiconductor Nb_3Cl_8. Nano Lett. **22**(11), 4596–4602 (2022)
47. S. Zhu, H. Liu, J. Wu, J. Mei, R. Zhang, Y. Liu, Y. Chen, K. Watanabe, T. Taniguchi, J. Meng, X. Cai, Tunable ambipolar transport in a 2D kagome semiconductor. Adv. Opt. Mater. **13**(2), 2402108 (2024)
48. Y. Song, T. Ying, X. Chen, X. Han, X. Wu, A.P. Schnyder, Y. Huang, J.-G. Guo, X. Chen, Competition of superconductivity and charge density wave in selective oxidized CsV_3Sb_5 thin flakes. Phys. Rev. Lett. **127**(23), 237001 (2021)

49. G. Zheng, C. Tan, Z. Chen, M. Wang, X. Zhu, S. Albarakati, M. Algarni, J. Partridge, L. Farrar, J. Zhou, W. Ning, M. Tian, M.S. Fuhrer, L. Wang, Electrically controlled superconductor-to-failed insulator transition and giant anomalous Hall effect in kagome metal CsV_3Sb_5 nanoflakes. Nat. Commun. **14**(1), 678 (2023)
50. M. Kang, S. Fang, L. Ye, H.C. Po, J. Denlinger, C. Jozwiak, A. Bostwick, E. Rotenberg, E. Kaxiras, J.G. Checkelsky, R. Comin, Topological flat bands in frustrated kagome lattice CoSn. Nat. Commun. **11**(1), 4004 (2020)
51. Z. Liu, M. Li, Q. Wang, G. Wang, C. Wen, K. Jiang, X. Lu, S. Yan, Y. Huang, D. Shen, J.X. Yin, Z. Wang, Z. Yin, H. Lei, S. Wang, Orbital-selective Dirac fermions and extremely flat bands in frustrated kagome-lattice metal CoSn. Nat. Commun. **11**(1), 4002 (2020)
52. J.X. Yin, N. Shumiya, S. Mardanya, Q. Wang, S.S. Zhang, H.J. Tien, D. Multer, Y. Jiang, G. Cheng, N. Yao, S. Wu, D. Wu, L. Deng, Z. Ye, R. He, G. Chang, Z. Liu, K. Jiang, Z. Wang, T. Neupert, A. Agarwal, T.R. Chang, C.W. Chu, H. Lei, M.Z. Hasan, Fermion-boson many-body interplay in a frustrated kagome paramagnet. Nat. Commun. **11**(1), 4003 (2020)
53. H. Tsai, T. Higo, K. Kondou, T. Nomoto, A. Sakai, A. Kobayashi, T. Nakano, K. Yakushiji, R. Arita, S. Miwa, Y. Otani, S. Nakatsuji, Electrical manipulation of a topological antiferromagnetic state. Nature **580**(7805), 608–613 (2020)
54. J.X. Yin, S.S. Zhang, H. Li, K. Jiang, G. Chang, B. Zhang, B. Lian, C. Xiang, I. Belopolski, H. Zheng, T.A. Cochran, S.Y. Xu, G. Bian, K. Liu, T.R. Chang, H. Lin, Z.Y. Lu, Z. Wang, S. Jia, W. Wang, M.Z. Hasan, Giant and anisotropic many-body spin-orbit tunability in a strongly correlated kagome magnet. Nature **562**(7725), 91–95 (2018)
55. M. Zhu, Q. Li, K. Guo, B. Chen, K. He, C. Yi, P. Lu, X. Li, J. Lu, J. Li, R. Wu, X. Liu, Y. Liu, L. Liao, B. Li, X. Duan, Two-dimensional ultrathin Fe_3Sn_2 kagome metal with defect-dependent magnetic property. Nano Lett. **24**(24), 7483–7490 (2024)
56. H. Inoue, M. Han, L. Ye, T. Suzuki, J.G. Checkelsky, Molecular beam epitaxy growth of antiferromagnetic kagome metal FeSn. Appl. Phys. Lett. **115**(7), 072403 (2019)
57. D. Hong, C. Liu, H.-W. Hsiao, D. Jin, J.E. Pearson, J.-M. Zuo, A. Bhattacharya, Molecular beam epitaxy of the magnetic kagome metal FeSn on $LaAlO_3$ (111). AIP Adv. **10**(10), 105017 (2020)
58. M. Han, H. Inoue S. Fang, J. Caolan, L. Ye, M.K. Chan, D. Graf, T. Suzuki, M.P. Ghimire, W.J. Cho, E. Kaxiras, J.G. Checkelsky, Evidence of two-dimensional flat band at the surface of antiferromagnetic kagome metal FeSn. Nat. Commun. **12**(1), 5345 (2021)
59. H. Zhang, B.D. Oli, Q. Zou, X. Guo, Z. Wang, L. Li, Visualizing symmetry-breaking electronic orders in epitaxial kagome magnet FeSn films. Nat. Commun. **14**(1), 6167 (2023)
60. H. Zhang, M. Weinert, L. Li, Giant periodic pseudomagnetic fields in strained kagome magnet FeSn epitaxial films on $SrTiO_3$ (111) substrate. Nano Lett. **23**(6), 2397–2404 (2023)
61. P.M. Laxmeesha, T.D. Tucker, R.K. Rai, S. Li, M.-W. Yoo, E.A. Stach, A. Hoffmann, S.J. May, Epitaxial growth and magnetic properties of kagome metal FeSn/elemental ferromagnet heterostructures. J. Appl. Phys. **135**(8), 085302 (2024)
62. L. Mosesso, L. Tomarchio, N. Bhattarai, S. Macis, P. Gori, A. Grilli, G.M. Cestelli, J. Philip, O. Pulci, S. Lupi, Evidence of high electron mobility in magnetic kagome topological metal FeSn thin films. Nanoscale Adv. **6**, 6378–6385 (2024)
63. Z. Ren, J. Huang, H. Tan, A. Biswas, A. Pulkkinen, Y. Zhang, Y. Xie, Z. Yue, L. Chen, F. Xie, K. Allen, H. Wu, Q. Ren, A. Rajapitamahuni, A.K. Kundu, E. Vescovo, J. Kono, E. Morosan, P. Dai, J.-X. Zhu, Q. Si, J. Minár, B. Yan, M. Yi, Persistent flat band splitting and strong selective band renormalization in a kagome magnet thin film. Nat. Commun. **15**(1), 9376 (2024)
64. D. Khadka, T.R. Thapaliya, J. Wen, R.F. Need, S.X. Huang, High quality epitaxial thin films and exchange bias of antiferromagnetic Dirac semimetal FeSn. Appl. Phys. Lett. **117**(3), 032403 (2020)
65. C.-F. Pai, Y. Ou, L.H. Vilela-Leão, D.C. Ralph, R.A. Buhrman, Dependence of the efficiency of spin Hall torque on the transparency of Pt/ferromagnetic layer interfaces. Phys. Rev. B **92**(6), 064426 (2015)
66. S. Sankar, R. Liu, C.-P. Zhang, Q.-F. Li, C. Chen, X.-J. Gao, J. Zheng, Y.-H. Lin, K. Qian, R.-P. Yu, X. Zhang, Z.Y. Meng, K.T. Law, Q. Shao, J. Berthold, Experimental evidence for a Berry curvature quadrupole in an antiferromagnet. Phys. Rev. X **14**(2), 021046 (2024)
67. Z. Ren H. Li S. Sharma D. Bhattarai, H. Zhao, B. Rachmilowitz, F. Bahrami, F. Tafti, S. Fang, M.P. Ghimire, Z. Wang, I. Zeljkovic, Plethora of tunable Weyl fermions in kagome magnet Fe_3Sn_2 thin films. npj Quantum Mater. **7**(1), 109 (2022)
68. S. Cheng, M. Nrisimhamurty, T. Zhou, N. Bagués, W. Zhou, A.J. Bishop, I. Lyalin, C. Jozwiak, A. Bostwick, E. Rotenberg, D.W. McComb, I. Žutić, R.K. Kawakami, Epitaxial kagome thin films as a platform for topological flat bands. Nano Lett. **23**(15), 7107–7113 (2023)
69. C. Chen, J. Zheng, R. Yu, S. Sankar, K.T. Law, H.C. Po, J. Berthold, Visualizing the localized electrons of a kagome flat band. Phys. Rev. Res. **5**(4), 043269 (2023)
70. S. Duan, J.-Y. You, J. Gou, J. Chen, Y.L. Huang, M. Liu, S. Sun, Y. Wang, X. Yu, L. Wang, Y.P. Feng, Y.-Y. Sun, A.T.S. Wee, W. Chen, Epitaxial growth of single-layer kagome nanoflakes with topological band inversion. ACS Nano **16**(12), 21079–21086 (2022)
71. S. Cheng, B. Liu, I. Lyalin, W. Zhou, J. Hwang, R.K. Kawakami, Atomic layer molecular beam epitaxy of kagome magnet RMn_6Sn_6 (R = Er, Tb) thin films. APL Mater. **12**(4), 041129 (2024)
72. M. Han, J. Caolan, J. Zheng, S. Fang, J.G. Checkelsky, Molecular beam epitaxy synthesis and electrical transport properties of the correlated kagome metal Ni_3In. Phys. Rev. B **109**(12), L121112 (2024)
73. J.S.R. McCoombs, B.D. MacNeil, V. Askarpour, J. Myra, H. Herdin, M. Pula, M.D. Robertson, G.M. Luke, K.L. Kavanagh, J. Maassen, T.L. Monchesky, Giant anomalous Hall effect in epitaxial $Mn_{3.2}Ge$ films with a cubic kagome structure. Phys. Rev. B **110**(6), 064401 (2024)
74. Y.E. Vekovshinin, L.V. Bondarenko, A.Y. Tupchaya, A.N. Mihalyuk, N.V. Denisov, D.V. Gruznev, A.V. Zotov, A.A. Saranin, Lifshitz transition in a single-atom-thick $Gd_xYb_{1-x}Pb_3$ kagome compound on Si(111). Nano Lett. **24**(32), 9931–9936 (2024)
75. Y.-H. Lin, C.-J. Chen, N. Kumar, T.-Y. Yeh, T.-H. Lin, S. Blügel, G. Bihlmayer, P.-J. Hsu, Fabrication and imaging monatomic Ni kagome lattice on superconducting Pb(111). Nano Lett. **22**(21), 8475–8481 (2022)
76. O. Kubo, S. Kinoshita, H. Sato, K. Miyamoto, R. Sugahara, S. Endo, H. Tabata, T. Okuda, M. Katayama, Kagome-like structure of germanene on Al(111). Phys. Rev. B **104**(8), 085404 (2021)
77. J.H. Lee, G.W. Kim, I. Song, Y. Kim, Y. Lee, S.J. Yoo, D.Y. Cho, J.-W. Rhim, J. Jung, G. Kim, C. Kim, Atomically thin two-dimensional kagome flat band on the silicon surface. ACS Nano **18**(37), 25535–25541 (2024)
78. K. Fujiwara, Y. Kato, T. Seki, K. Nomura, K. Takanashi, Y. Motome, A. Tsukazaki, Tuning scalar spin chirality in ultrathin films of the kagome-lattice ferromagnet Fe_3Sn. Commun. Mater. **2**(1), 113 (2021)
79. S. Kurosawa, T. Higo, S. Saito, R. Uesugi, S. Nakatsuji, Large spontaneous magneto-thermoelectric effect in epitaxial thin films of the topological kagome ferromagnet Fe_3Sn. Phys. Rev. Mater. **8**(5), 054206 (2024)
80. K.I.A. Khan, A. Kumar, P. Gupta, R.S. Yadav, J. Åkerman, P.K. Muduli, Magnetodynamic properties of ultrathin films of Fe_3Sn_2 - a topological kagome ferromagnet. Sci. Rep. **14**(1), 3487 (2024)
81. D. Khadka, T.R. Thapaliya, P.S. Hurtado, J. Wen, R. Need, J.M. Kikkawa, S.X. Huang, Anomalous Hall and Nernst effects in epitaxial films of topological kagome magnet Fe_3Sn_2. Phys. Rev. Mater. **4**(8), 084203 (2020)
82. K.I.A. Khan, R.S. Yadav, H. Bangar, A. Kumar, N. Chowdhury, P.K. Muduli, P.K. Muduli, Intrinsic anomalous Hall effect in thin films of topological kagome ferromagnet Fe_3Sn_2. Nanoscale **14**(23), 8484–8492 (2022)
83. D. Zhang, Z. Hou, W. Mi, Anomalous and topological Hall effects of ferromagnetic Fe_3Sn_2 epitaxial films with kagome lattice. Appl. Phys. Lett. **120**(23), 232401 (2022)
84. J. Ikeda, K. Fujiwara, J. Shiogai, T. Seki, K. Nomura, K. Takanashi, A. Tsukazaki, Critical thickness for the emergence of Weyl features in $Co_3Sn_2S_2$ thin films. Commun. Mater. **2**(1), 18 (2021)
85. T.R. Thapaliya, T. Yoo, P.S. Hurtado, N.D. Arndt, R.F. Need, J.M. Kikkawa, H. Kim, S.X. Huang, High-quality epitaxial thin films of topological kagome metal CoSn by magnetron sputtering. Appl. Phys. Lett. **119**(20), 201902 (2021)
86. K. Fujiwara, Y. Kato, H. Abe, S. Noguchi, J. Shiogai, Y. Niwa, H. Kumigashirai, Y. Motome, A. Tsukazaki, Berry curvature contributions of kagome-lattice fragments in amorphous Fe–Sn thin films. Nat. Commun. **14**(1), 3399 (2023)
87. D. Hong, N. Anand, C. Liu, H. Liu, I. Arslan, J.E. Pearson, A. Bhattacharya, J.S. Jiang, Large anomalous Nernst and inverse spin-Hall effects in epitaxial thin films of kagome semimetal Mn_3Ge. Phys. Rev. Mater. **4**(9), 094201 (2020)
88. Y. Takeuchi, Y. Yamane, J.-Y. Yoon, R. Itoh, B. Jinnai, S. Kanai, J. Ieda, S. Fukami, H. Ohno, Chiral-spin rotation of non-collinear antiferromagnet by spin–orbit torque. Nat. Mater. **20**(10), 1364–1370 (2021)
89. M. Raju, R. Romero, D. Nishio-Hamane, R. Uesugi, M. Asakura, Z. Tagay, T. Higo, N.P. Armitage, C. Broholm, S. Nakatsuji, Anisotropic anomalous

transport in the kagome-based topological antiferromagnetic Mn_3Ga epitaxial thin films. Phys. Rev. Mater. **8**(1), 014204 (2024)
90. B. Song, T. Ying, X. Wu, W. Xia, Q. Yin, Q. Zhang, Y. Song, X. Yang, J. Guo, L. Gu, X. Chen, J. Hu, A.P. Schnyder, H. Lei, Y. Guo, S. Li, Anomalous enhancement of charge density wave in kagome superconductor CsV_3Sb_5 approaching the 2D limit. Nat. Commun. **14**(1), 2492 (2023)
91. H.-X. Lou, X.-G. Ye, X. Liao, T.-Y. Zhao, A.-Q. Wang, D.-P. Yu, Z.-M. Liao, Resistive anisotropy in the charge density wave phase of kagome superconductor CsV_3Sb_5 thin films. Appl. Phys. Lett. **125**(13), 132601 (2024)
92. N. Doudin, K. Saritas, M. Li, I. Ennen, J.A. Boscoboinik, P. Dementyev, A. Hütten, S. Ismail-Beigi, E.I. Altman, Twisting and rippling of a two-dimensional kagome lattice: silica on Au(111). ACS Mater. Lett. **4**(9), 1660–1667 (2022)
93. H. Zhang, Q. Liu, L. Deng, Y. Ma, S. Daneshmandi, C. Cen, C. Zhang, P.M. Voyles, X. Jiang, J. Zhao, C.-W. Chu, Z. Gai, L. Li, Room-temperature ferromagnetism in epitaxial bilayer $FeSb/SrTiO_3(001)$ terminated with a kagome lattice. Nano Lett. **24**(1), 122–129 (2023)
94. S. Duan, J.-Y. You, Z. Cai, J. Gou, D. Li, Y.L. Huang, X. Yu, S.L. Teo, S. Sun, Y. Wang, M. Lin, C. Zhang, B. Feng, A.T.S. Wee, C. Wei, Observation of kagome-like bands in two-dimensional semiconducting Cr_8Se_{12}. Nat. Commun. **15**(1), 8940 (2024)
95. Z. Li, J. Zhuang, L. Wang, H. Feng, Q. Gao, X. Xu, W. Hao, X. Wang, C. Zhang, K. Wu, S.X. Dou, L. Chen, Z. Hu, Y. Du, Realization of flat band with possible nontrivial topology in electronic kagome lattice. Sci. Adv. **4**(11), eaau4511 (2018)
96. L. Lei, J. Dai, H. Dong, Y. Geng, F. Cao, C. Wang, R. Xu, F. Pang, Z.-X. Liu, F. Li, Z. Cheng, G. Wang, W. Ji, Electronic Janus lattice and kagome-like bands in coloring-triangular $MoTe_2$ monolayers. Nat. Commun. **14**(1), 6320 (2023)
97. S. Park, S. Kang, H. Kim, K.H. Lee, P. Kim, S. Sim, N. Lee, B. Karuppannan, J. Kim, J. Kim, K.I. Sim, M.J. Coak, Y. Noda, C.H. Park, J.H. Kim, J.G. Park, Kagome van-der-Waals $Pd_3P_2S_8$ with flat band. Sci. Rep. **10**(1), 20998 (2020)
98. H. Liu, W. Li, Z. Zhou, H. Qu, J. Zhang, W. Hu, C. Wen, N. Wang, H. Deng, G. Li, S. Yan, Direct evidence of intrinsic Mott state and its layer-parity oscillation in a breathing kagome crystal down to monolayer. Phys. Rev. Lett. **135**(7), 076503 (2025)
99. D. Dettmann, P.M. Sheverdyaeva, E. Hamzehpoor, S. Franchi, G. Galeotti, P. Moras, C. Ceccarelli, D.F. Perepichka, F. Rosei, G. Contini, Electronic band engineering of two-dimensional kagomé polymers. ACS Nano **18**(1), 849–857 (2023)
100. Z. Shi, N. Lin, Porphyrin-based two-dimensional coordination kagome lattice self-assembled on a Au(111) surface. J. Am. Chem. Soc. **131**(15), 5376–5377 (2009)
101. W.-C. Pan, C. Mützel, S. Haldar, H. Hohmann, S. Heinze, J.M. Farrell, R. Thomale, M. Bode, F. Würthner, J. Qi, Diboraperylene diborinic acid self-assembly on Ag(111)—kagome flat band localized states imaged by scanning tunneling microscopy and spectroscopy. Angew. Chem. **63**(15), e202400313 (2024)
102. U. Schlickum, R. Decker, F. Klappenberger, G. Zoppellaro, S. Klyatskaya, W. Auwärter, S. Neppl, K. Kern, H. Brune, M. Ruben, J.V. Barth, Chiral kagomé lattice from simple ditopic molecular bricks. J. Am. Chem. Soc. **130**(35), 11778–11782 (2008)
103. R. Yin, X. Zhu, Q. Fu, T. Hu, L. Wan, Y. Wu, Y. Liang, Z. Wang, Z.-L. Qiu, Y.-Z. Tan, C. Ma, S. Tan, W. Hu, B. Li, Z.F. Wang, J. Yang, B. Wang, Artificial kagome lattices of Shockley surface states patterned by halogen hydrogen-bonded organic frameworks. Nat. Commun. **15**(1), 2969 (2024)
104. G. Galeotti, F. De Marchi, E. Hamzehpoor, O. MacLean, M. Rajeswara Rao, Y. Chen, L.V. Besteiro, D. Dettmann, L. Ferrari, F. Frezza, P.M. Sheverdyaeva, R. Liu, A.K. Kundu, P. Moras, M. Ebrahimi, M.C. Gallagher, F. Rosei, D.F. Perepichka, G. Contini, Synthesis of mesoscale ordered two-dimensional π-conjugated polymers with semiconducting properties. Nat. Mater. **19**(8), 874–880 (2020)
105. I. Lyalin, S. Cheng, R.K. Kawakami, Spin-orbit torque in bilayers of kagome ferromagnet Fe_3Sn_2 and Pt. Nano Lett. **21**(16), 6975–6982 (2021)
106. J. Wang, Y. Zheng, X. Nie, C. Xu, Z. Hao, L. Song, S. You, J. Xi, M. Pan, H. Lin, Y. Li, H. Zhang, Q. Li, L. Chi, Constructing and transferring two-dimensional tessellation kagome lattices via chemical reactions on Cu(111) surface. J. Phys. Chem. Lett. **12**(34), 8151–8156 (2021)
107. R. Ilan, A.G. Grushin, D.I. Pikulin, Pseudo-electromagnetic fields in 3D topological semimetals. Nat. Rev. Phys. **2**(1), 29–41 (2020)
108. H. Zhang, Z. Wang, M. Weinert, L. Li, Anisotropic response of defect bound states to the magnetic field in epitaxial FeSn films. Nano Lett. **25**(12), 4689–4695 (2025)
109. X. Zhang, Q. Lu, W. Liu, W. Niu, J. Sun, J. Cook, M. Vaninger, P.F. Miceli, D.J. Singh, S.-W. Lian, T.-R. Chang, X. He, J. Du, L. He, R. Zhang, G. Bian, Y. Xu, Room-temperature intrinsic ferromagnetism in epitaxial $CrTe_2$ ultrathin films. Nat. Commun. **12**(1), 2492 (2021)
110. Y. Cai, Z. Hao, L. Wang, Y. Wang, Y. Liu, J.-W. Mei, J. Wang, C. Chen, Angle-resolved photoemission spectroscopy study on kagome superconductor AV_3Sb_5 (A = K, Rb, Cs). Supercond. Sci. Technol. **37**(12), 123001 (2024)
111. J. Yang, J. Huang, L. Zhao, X.J. Zhou, Angle-resolved photoemission spectroscopy study on transition-metal kagome materials. Chin. Phys. B **34**(4), 047101 (2025)
112. S.E. Clifton, Collective electron ferromagnetism. Proc. R. Soc. Lond. Ser. A, Math. Phys. Sci. **165**(922), 372–414 (1938)
113. M. Pickel, A.B. Schmidt, M. Weinelt, M. Donath, Magnetic exchange splitting in Fe above the Curie temperature. Phys. Rev. Lett. **104**(23), 237204 (2010)
114. F. Pollmann, P. Fulde, K. Shtengel, Kinetic ferromagnetism on a kagome lattice. Phys. Rev. Lett. **100**(13), 136404 (2008)
115. Z. Lin, C. Wang, P. Wang, S. Yi, L. Li, Q. Zhang, Y. Wang, Z. Wang, H. Huang, Y. Sun, Dirac fermions in antiferromagnetic FeSn kagome lattices with combined space inversion and time-reversal symmetry. Phys. Rev. B **102**(15), 155103 (2020)
116. M. Yi, Z.K. Liu, Y. Zhang, R. Yu, J-X. Zhu, J.J. Lee, R.G. Moore, F.T. Schmitt, W. Li, S.C. Riggs, Observation of universal strong orbital-dependent correlation effects in iron chalcogenides. Nat. Commun. **6**(1), 7777 (2015)
117. J. Huang, R. Yu, Z. Xu, J.-X. Zhu, J.S. Oh, Q. Jiang, M. Wang, H. Wu, T. Chen, J.D. Denlinger, Correlation-driven electronic reconstruction in $FeTe_{1-x}Se_x$. Commun. Phys. **5**(1), 29 (2022)
118. S-C. Wang, H-B. Yang, A.K.P. Sekharan, H. Ding, J.R. Engelbrecht, X. Dai, Z. Wang, A. Kaminski, T. Valla, T. Kidd, Quasiparticle line shape of Sr_2RuO_4 and its relation to anisotropic transport. Phys. Rev. Lett. **92**(13), 137002 (2004)
119. T.E. Kidd, T. Valla, A.V. Fedorov, P.D. Johnson, R.J. Cava, M.K. Haas, Orbital dependence of the Fermi liquid state in Sr_2RuO_4. Phys. Rev. Lett. **94**(10), 107003 (2005)
120. A.Y. Tupchaya, L.V. Bondarenko, Y.E. Vekovshinin, A.A. Yakovlev, A.N. Mihalyuk, D.V. Gruznev, C.R. Hsing, C.M. Wei, A.V. Zotov, A.A. Saranin, Double-atomic-layer Tl-Mg compound on a Si(111) surface with advanced electronic properties. Phys. Rev. B **101**(23), 235444 (2020)
121. M. Pan, X. Zhang, Y. Zhou, P. Wang, Q. Bian, H. Liu, X. Wang, X. Li, A. Chen, X. Lei, S. Li, Z. Cheng, Z. Shao, H. Ding, J. Gao, F. Li, F. Liu, Growth of mesoscale ordered two-dimensional hydrogen-bond organic framework with the observation of flat band. Phys. Rev. Lett. **130**(3), 036203 (2023)

Publisher's note